Engineering Structures 102 (2015) 156–175

Contents lists available at ScienceDirect

Engineering Structures

journal homepage: www.elsevier.com/locate/engstruct

Simplified analytical solution for axial load capacity of concrete-filled double-skin tube (CFDST) columns subjected to fire

R. Imani [a,*], M. Bruneau [a], G. Mosqueda [b]

[a] Dept. of Civil, Structural and Environmental Engineering, Univ. at Buffalo, Buffalo, NY 14260, United States
[b] Dept. of Structural Engineering, University of California at San Diego, La Jolla, CA 92093, United States

ARTICLE INFO

Article history:
Received 9 December 2014
Revised 2 August 2015
Accepted 3 August 2015

Keywords:
Concrete-filled double-skin tube (CFDST) columns
Composite columns
Fire resistance
Thermal-stress problem
Analytical solution
Fire-resistant design

ABSTRACT

Concrete-filled steel tube (CFST) columns and even more so concrete-filled double-skin tube (CFDST) columns have demonstrated a desirable behavior when subjected to fire loading conditions. Current methods to estimate the axial load capacity for these columns exposed to fire are either limited to simple cases using tables or require complex finite element analysis. In an effort to develop a more general and practical approach to this problem, a simplified step by step analytical procedure is proposed for the calculation of the axial load capacity of CFDST columns subjected to any given time–temperature (fire) curve. The procedure was defined by combining an analytical solution to the heat transfer problem with calculation of axial load capacity using the fire-modified material properties adopted from the Eurocode 4 general rules for structural fire design. The proposed method was verified with existing experimental and advanced finite element simulation results. A number of design recommendations, based on the knowledge gained from using the procedure for different case studies, are proposed for CFDST columns subjected to fire.

1. Introduction

Several past studies have demonstrated a promising behavior for concrete filled steel tube (CFST) columns subjected to extreme events including seismic [1–4], and fire [5–9] conditions. More recently, an enhanced type of CFST columns, termed concrete filled double-skin tube (CFDST) columns consisting of concrete between an outer and inner steel tube, have also demonstrated a desirable performance under separate seismic loading [10–12] and fire conditions [13–15]. Furthermore, Imani et al. demonstrated that CFDST columns can retain nearly all of their undamaged fire resistance capacity after being subjected to significant seismic damage [16]. This promising performance of CFSTs and CFDSTs in fire highlights the need for a simplified calculation method for estimating their fire resistance (as opposed to relying on finite element analysis), particularly from a design perspective where simple but rapid and sufficiently accurate strength calculations are crucial.

After reviewing existing methods for calculation of the fire resistance of axially loaded CFDST columns, this paper presents a new simplified two-step procedure. The first step provides an analytical based solution for the heat transfer problem, which calculates the temperature distribution for the CFDST column cross-section based on a given fire (time–temperature) curve. The second step uses selected results from the first step to calculate the design axial load capacity of the CFDST column at any particular time during the application of the time–temperature curve. Note that the procedure is defined for CFDST columns, but can also be used for the traditional CFST cases, with slight modifications.

2. Background

With respect to the performance of CFST columns under fire conditions, several methods have already been developed (based on both experimental and numerical studies) to calculate their fire resistance time. Han et al. [7] proposed one such equation for unprotected CFST columns based on regression analyses of experimental results. Another method by Kodur and MacKinnon [17] uses a single empirical equation to calculate the fire resistance of axially loaded CFST columns.

Eurocode 4 provides three calculation methods for the design of CFST columns under fire [4]: the first approach (i.e., tabulated values of axial load capacity for a few common cases of concrete filled columns) is limited to a few cases (both in terms of the column geometry and the applied fire curve), and is not applicable to a CFDST column or for any column subjected to a general fire curve;

* Corresponding author.
E-mail addresses: rezaiman@buffalo.edu (R. Imani), bruneau@buffalo.edu (M. Bruneau), gmosqueda@ucsd.edu (G. Mosqueda).

http://dx.doi.org/10.1016/j.engstruct.2015.08.007
0141-0296/

the second method (referred to as simple calculation method in Eurocode), provides a step by step procedure to calculate the fire resistance time by incrementally increasing the uniformly distributed strain of the section to satisfy the axial equilibrium using the material properties modified for elevated temperatures; however, it assumes that the designer knows the temperature distribution within the cross-section at any particular time during the fire exposure, even though no simplified method is given in Eurocode to calculate this temperature field; the third method requires an advanced nonlinear thermal-stress finite element analysis.

Espinos et al. [18] proposed a method for calculating a uniform equivalent temperature for the whole concrete core (and similarly another one for the steel tube), which if used in the Eurocode method, will provide the same fire resisting time as the one obtained considering the actual non-uniform temperature distribution. The uniform temperature value was conservatively determined to be the maximum of two values, which were calculated such as to produce the same axial force resistance (assuming a fully plastic section) and flexural stiffness for the cross-section as for the case with true non-uniform temperature distribution. After conducting fire resistance time analyses using this procedure for several different CFST columns, two equations were proposed based on regression analyses, for calculating of the equivalent uniform temperature for the steel tube and concrete core, namely:

$$T_{s,eq} = 342.1 + 10.77R - 0.044R^2 + 3.922A_m/V - 0.025RA_m/V \quad (1)$$

$$T_{c,eq} = -186.44 + 5.764R - 0.026R^2 + 22.577A_m/V - 0.32(A_m/V)^2 + 0.14RA_m/V \quad (2)$$

In these equations, $T_{s,eq}, T_{c,eq}$ are the equivalent uniform temperature values for the steel and concrete sections, and the section factor, A_m/V, is the ratio of the surface area of the steel tube to its volume. The expression for the section factor can be simplified to $4/D$, in which D is the outer diameter of the steel tube. The parameter R, in both equations, refers to the standard fire resistance class, which is given as 30, 60, 90, and 120 for standard resistance times of 30, 60, 90 and 120 min. Although Eqs. (1) and (2) were shown to provide acceptable results for CFST columns with different cross-sections, they were limited to the case of exposure to the standard ASTM E119 fire [19], and (most importantly) there were no CFDST columns in the database used in the regression analysis.

This study builds upon and enhances the second method (referred to as simple calculation method in Eurocode), which is more practical than finite element analyses and can be applied to more general cases. The proposed simplified method presents an approach for calculation of temperature field, in which the well-known general mathematic solution for the heat transfer problem is tailored to specific needs of the problem at hand (i.e. making the solution directly applicable to any general form of fire curves), and simplified for engineering calculation while keeping it accurate enough for the purposes of this study. Moreover, the simplified method proposed in this paper modifies the Eurocode trial and error method for calculation of axial load capacity by introducing a procedure that limits the number of steps to less than four in the worst cases.

3. Analytical solution for the heat transfer problem

3.1. General solution for heat conduction differential equation

The objective of this section is to analytically solve the heat conduction partial differential equation for the cross-section of any given CFDST column. The cross-section is initially at room temperature, T_0, and its outer edge is subjected to a predetermined time–temperature curve, $f(t)$. Fig. 1a shows the cross section of a CFDST column. Considering the relatively higher heat conductivity of steel compared to concrete (about 10 times larger), it is assumed that both the outer and inner steel tube sections have a uniform temperature distribution with the outer tube temperature equal to $f(t)$. Based on this assumption, the temperature distribution problem can be reduced to a single material model for the cylindrical concrete section subjected to $f(t)$ (Fig. 1b).

Considering a polar coordinate system, the boundaries of the section are defined by r_o (radius of the outer tube) and r_i (radius of the inner tube), with a specific point in the cross section referenced by (r,θ). The differential equation of heat conduction for the cylindrical section can be written as [20]:

$$\alpha^2\left(u_{,rr} + \frac{1}{r}u_{,r} + \frac{1}{r^2}u_{,\theta\theta}\right) = u_{,t} \quad r_i \leqslant r \leqslant r_o,\ 0 \leqslant \theta \leqslant 2\pi,\ 0 \leqslant t < \infty$$
$$u(r,\theta,0) = T_0, \quad u(r_o,\theta,t) = f(t) \quad (3)$$

where $u(r,\theta,t)$ is the temperature field in the section, $u_{,r} = \frac{\partial u}{\partial r}, u_{,rr} = \frac{\partial^2 u}{\partial r^2}, u_{,\theta\theta} = \frac{\partial^2 \theta}{\partial \theta^2}$ and $u_{,t} = \frac{\partial u}{\partial t}$. The initial condition is defined by $u(r,\theta,0) = T_0$ and the boundary condition for the exposed outer edge is given by $u(r_o,\theta,t) = f(t)$. The thermal diffusivity of the material, α^2, is given by:

$$\alpha^2 = \frac{k}{\rho c_p} \quad (4)$$

in which k is the thermal conductivity, ρ is density, and c_p is the specific heat capacity of the material. Although these three parameters can vary with temperature, the differential equation is solved assuming a constant α^2 (using constant values recommended in Eurocode). Potential effects of this assumption on the accuracy of the solution is examined in the verification study presented in Section 3.3.

Since the domain is cylindrical and the column is assumed to be fully surrounded by the heat source (i.e., the temperature distribution is assumed to be uniform at all points on the cylindrical surface, the initial conditions and boundary conditions are both independent of θ and therefore, the resulting temperature field, u, is independent of θ and a function only of r and t). Note that in real fires, distribution of temperature can also change along the height of the column because the fire exposure is not usually uniform in all locations. The equations here assume a uniform surrounding fire, which causes a uniform temperature increase at all locations on the outer surface of column. Therefore, results are expected to be conservative.

If the equation is solved for values of r in the region, $r_i = 0 \leqslant r \leqslant r_o$, it can be used for all the other cases that have the configuration $0 < r_i \leqslant r \leqslant r_o$. Therefore, the differential equation is solved for a circular section, providing a general solution that can be used for both CFST and CDFST columns. In case of a CFDST section, the temperature at the radius, r_i, is taken as the temperature of the inner tube, and all temperature values for radius values below r_i are irrelevant. Applying these modifications to Eq. (3), the governing differential equation is simplified to:

$$\alpha^2\left(u_{,rr} + \frac{1}{r}u_{,r}\right) = u_{,t} \quad 0 = r_i \leqslant r \leqslant r_o,\ 0 \leqslant t < \infty$$
$$u(r,0) = T_0, \quad u(r_o,t) = f(t) \quad (5)$$

Note that the term $u_{\theta\theta}$ is eliminated. The partial differential equation has a boundary condition which is non-homogeneous only in time ($u(r_o,t) = f(T)$) and can be solved according to procedures given in various advanced engineering mathematics textbooks (e.g. [20]). Although the mathematical solution is well

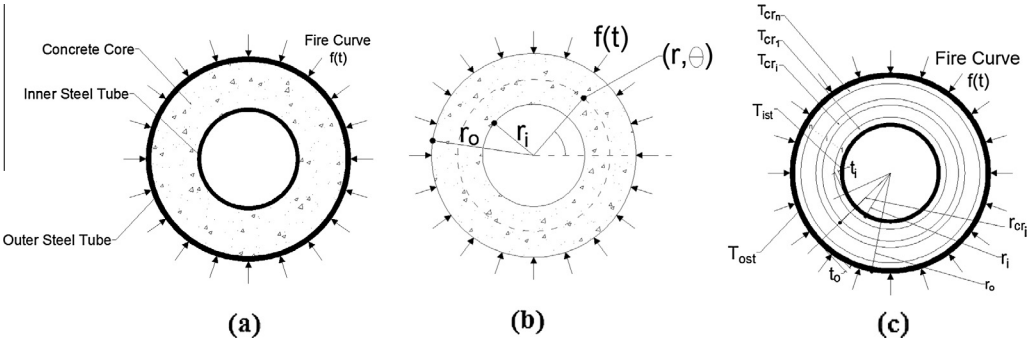

Fig. 1. Cross-section of a CFDST column for the thermal/structural problem: (a) with steel tubes; (b) without steel tubes (assuming uniform temperature for steel sections); (c) steel and concrete regions with uniform temperature distribution.

known, it is briefly presented here to show the path to the main resulting equation which will be used as the basis of simplified equations in the latter parts of this paper. The solution (i.e., $u(r,t)$) can be written as the summation of:

$$u(r,t) = u_0(r,t) + v(r,t) \tag{6}$$

in which $u_0(r,t)$ is a function satisfying only the non-homogeneous boundary condition, $u_0(r_o,t) = f(t)$. To fulfill this requirement, it is assumed that $u_0(r,t) = f(T)$. As a result:

$$u_{,r} = v_{,r} \tag{7}$$
$$u_{,rr} = v_{,rr} \tag{8}$$
$$u_{,t} = v_{,t} + f'(t) \tag{9}$$
$$u(r,0) = f(0) + v(r,0) = T_0 \tag{10}$$
$$u(r_o,t) = f(T) + v(r_o,t) = f(t) \tag{11}$$

Assuming that $f(t)$ is the specified time–temperature curve starting at room temperature, it is inferred that $f(0) = T_0$. Adding this information to Eq. (10) gives:

$$v(r,0) = 0 \tag{12}$$

Also from Eq. (11):

$$v(r_o,t) = 0 \tag{13}$$

Using Eqs. (8)–(13) new problem can be defined for the function $v(r,t)$ as:

$$\alpha^2\left(v_{,rr} + \frac{1}{r}v_{,r}\right) = v_{,t} + f'(t) \quad 0 = r_i \leqslant r \leqslant r_o,\ 0 \leqslant t < \infty$$
$$v(r,0) = 0, \quad v(r_o,t) = 0 \tag{14}$$

Using the method of separation of variables, as presented in Appendix A, the solution to Eq. (14) can be written as:

$$u(r,t) = v(r,t) + u_0(r,t)$$
$$u(r,t) = \left[\underbrace{\sum_{n=1}^{\infty}\left[\int_0^t \frac{2(-f'(\tau))}{z_n J_1(z_n)} e^{\left(\frac{z_n\alpha}{r_o}\right)^2\tau} d\tau\right]}_{I^*} J_0\left(z_n\frac{r}{r_o}\right)e^{-\left(\frac{z_n\alpha}{r_o}\right)^2 t}\right] + f(t) \tag{15}$$

in which J_0 and J_1 are Bessel functions of the first type and z_n's are the n first positive roots of the Bessel function $J_0(z)$. Eq. (15) can be used to calculate the temperature of a point, located at the radial distance r from the center of a circular region, which is subjected to a time–temperature (fire) curve of $f(t)$ along its outer edge. Although Eq. (15) provides the exact solution for the heat transfer problem, its implementation requires the use of advanced mathematical tools. A number of simplifications are presented in the following section to make Eq. (15) more suitable for simple hand calculations.

3.2. Simplification of the solution for heat transfer problem for practical purposes

The first step in the simplification of Eq. (15) is to limit the number of terms that need to be included in the summation that is part of the equation, provided that the results remain sufficiently accurate for the purposes of this study. Comparison of results obtained considering various number of terms in the summation revealed that the equation can provide acceptable results when the first four terms are included in the summation. Including four terms requires the use of the first four positive roots of $J_0(z)$, namely $z_1 = 2.405, z_2 = 5.520, z_3 = 8.654$ and $z_4 = 11.792$. Knowing the values of z_1 to z_4, it is possible to calculate the numerical values of the first four terms of $J_1(z_n)$, and include them as constants in the final formula. The term, $J_0\left(z_n\frac{r}{r_o}\right)$ must be calculated specifically for a given column's dimensions and cannot be turned into a set of constants. The function, $J_0(z)$, is defined by the infinite series:

$$J_0(z) = 1 - \frac{z^2}{(1!)^2 2^2} + \frac{z^4}{(2!)^2 2^4} - \frac{z^6}{(3!)^2 2^6} + \cdots \tag{16}$$

For values of $z > 1$, the function $J_0(z)$ can be approximated using the formula:

$$J_0(z) \cong \left(\sqrt{\frac{2}{\pi z}}\right)\cos\left(z - \frac{\pi}{4}\right) \tag{17}$$

Fig. 2a compares the results of the two formulas (Eqs. (16) and (17)) for positive values of z. Since the approximate formula (Eq. (17)) diverges from exact results for the values of $z < 1$, an additional linear approximation was defined for that region shown by the dotted line in Fig. 2a. Combining the two approximate formulas, numerical values of $J_0(z)$ can be obtained from:

$$J_0(z) \cong \begin{cases} 1 - 0.2349z, & z \leqslant 1 \\ \left(\sqrt{\frac{2}{\pi z}}\right)\cos\left(z - \frac{\pi}{4}\right), & z \geqslant 1 \end{cases} \tag{18}$$

The next step in the simplification of Eq. (15) is to calculate the integral term I^* (defined in Eq. (15)), which requires the first derivative of the applied fire curve. Assuming that any given fire curve, $f(t)$, can be approximated by a piecewise linear function, its first derivative would have constant values over the corresponding regions. This allows the term $(-f'(t))$ to be extracted from the integral as a constant, thus simplifying the calculations.

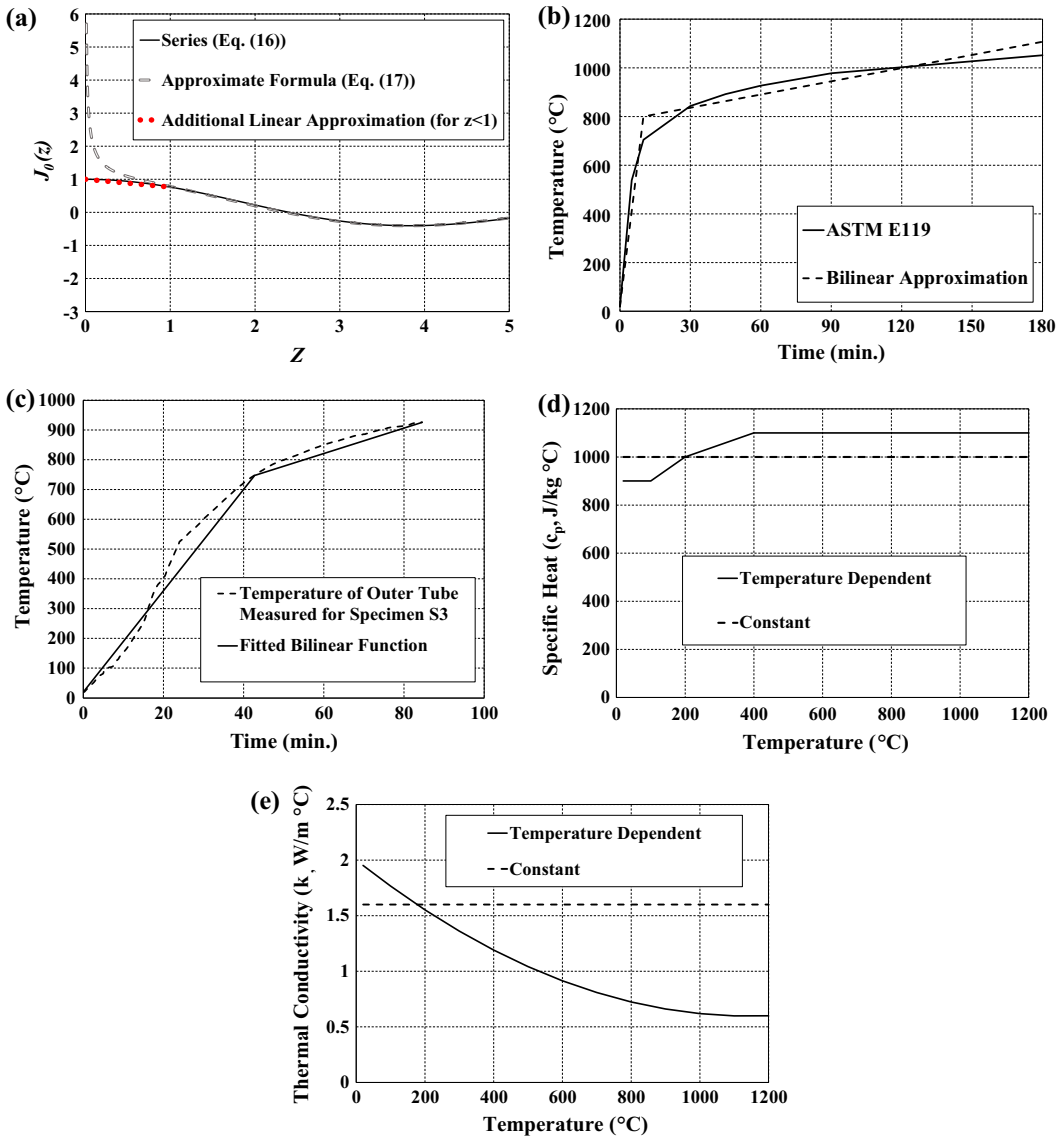

Fig. 2. Comparison of the exact and approximated (i.e. fitted functions or assumed constant values): (a) $\boldsymbol{J_0(z)}$ function; (b) ASTM E119 standard fire curve; (c) time–temperature curve measured for the outer tube of specimen S3; (d) concrete specific heat [4]; (e) concrete thermal conductivity [4].

For the purposes of this study, the function $f(t)$ initiating at room temperature T_0 is defined as a bilinear approximation of the given fire curve expressed as:

$$f(t) = \begin{cases} a_1 t + T_0, & t \leqslant t_1 \\ a_2 t + b_2, & t \geqslant t_1 \end{cases} \tag{19}$$

in which a_1, a_2, and b_2 are constants defined to provide the best fit for the fire curve. Note that for more sophisticated cases, where a bilinear approximation might be insufficient, multiple linear segments can be defined to follow the given fire curve with more accuracy. Using Eq. (19), the first derivative of the function is given by:

$$f'(t) = \begin{cases} a_1, & t \leqslant t_1 \\ a_2, & t \geqslant t_1 \end{cases} \tag{20}$$

As an example, a bilinear function can be defined to represent the standard ASTM E119 fire curve in °C and t in min. as:

$$f_{ASTM\ E119}(t) = \begin{cases} 78t + 20, & t \leqslant 10\ \text{min}. \\ 1.8t + 783.2, & t \geqslant 10\ \text{min}. \end{cases} \tag{21}$$

Fig. 2b shows the ASTM E119 Standard fire curve along with the approximate bilinear function. Since this fire curve has an initial sharp increasing branch followed by a second part over which temperature increases at a much slower rate, the bilinear function provides a reasonable approximation. Note that Eq. (21) was selected as a simple bilinear approximation to demonstrate the procedure. In this case, temperature values are greater than the standard curve in the first 30 min (i.e. the steep segment) and within the ±5% of standard curve temperature in the second segment. However, any other piecewise linear function can be used as a fire curve following a similar approach to obtain more conservative or accurate results. The proposed bilinear approximation for the ASTM E119 standard fire curve gives the following values for the first derivative:

$$f'_{ASTM\ E119}(t) = \begin{cases} a_1 = 78, & t < 10\ \text{min}. \\ a_2 = 1.8, & t > 10\ \text{min}. \end{cases} \tag{22}$$

Assuming that the function, $f(t)$, is bilinear, as presented in Appendix A, Eq. (15) can be simplified as:

$$u_{bilinear\ fire}(r,t) = \frac{r_o^2}{\alpha^2}[-0.2770A_1(t)B_1(t) + 0.0349A_2(t)B_2(t) - 0.0114A_3(t)B_3(t) + 0.0052A_4(t)B_4(t)] + f(t) \quad (23)$$

All parameters used in Eq. (23) are summarized in Table 1. In this equation, r_o is the radius of a circular section (or the outer radius of a cylindrical section), r is the radial distance of any selected point in the section and t is the amount of time (in minutes) past from the start of the exposure of the circular section's outer edge to the bilinear fire curve, $f(t)$. Using these parameters, $u_{bilinear\ fire}(r,t)$ can be calculated as the temperature of the selected point at the selected time. For simplicity in the sections that follow, Eq. (23), defining the temperature distribution in a cross-section of a CFDST column exposed to a bilinear fire curve will be referred to as $u(r,t)$ (instead of $u_{bilinear\ fire}(r,t)$).

To keep the solution adequately simple for engineering applications, Eq. (23) only accounts for the conduction mechanism, thus neglecting the effects of convection and radiation. This simplification, along with the assumption of a uniform temperature through the thickness of outer and inner tubes, may limit the accuracy of the solution. In real conditions, convection and radiation mechanisms play an important role in the transfer of thermal energy from the fire source to the outer surface of the column. However, the solution presented here starts with the assumption that the time-history of temperature on the surface of the outer tube is known (and used as a boundary condition), thus bypassing the heat transfer process through convection and radiation. Note that for the verification studies described below, the time–temperature curve for the surface of the outer steel tube was known and can be used directly in the solution. For real cases, in which only the fire source temperature is known, the method should be used by applying the source temperature directly to the surface of the steel tube (bypassing the convection and radiation mechanisms in the process). This, along with the assumption of a similar temperature for the inner and outer surfaces of the steel tube, ensures that the loss of accuracy due to the above model simplifications will lead to conservative results. Moreover, note that radiation and convection effects inside the CFDST column are considered to be negligible, an assumption that seemed adequate for the case studies presented below, but could be further verified against other experimental or numerical results in future research.

Table 1
Summary of the parameters needed for the calculation of the temperature field using Eq. (23).

Parameter/function	Expression
$A_n(t), n = 1\ to\ 4$	$A(t) = \begin{cases} a_1\left[e^{\left(\frac{2n\alpha}{r_o}\right)^2 t} - 1\right], & t \leqslant t_1 \\ a_1\left[e^{\left(\frac{2n\alpha}{r_o}\right)^2 t_1} - 1\right] + a_2\left[e^{\left(\frac{2n\alpha}{r_o}\right)^2 t} - e^{\left(\frac{2n\alpha}{r_o}\right)^2 t_1}\right], & t > t_1 \end{cases}$
$B_n(t), n = 1\ to\ 4$	$B_n(t) = \left[e^{-\left(\frac{2n\alpha}{r_o}\right)^2 t}\right]\left[\begin{cases} 1 - 0.2349z_n^*, & z_n^* = z_n\frac{r}{r_o} \leqslant 1 \\ \sqrt{\frac{2}{\pi z_n^*}}Cos(z_n^* - \frac{\pi}{4}), & z_n^* = z_n\frac{r}{r_o} \geqslant 1 \end{cases}\right]$
$f(t)$ (Bilinear fire curve applied to the outer edge)	$f(t) = \begin{cases} a_1 t + T_0, & t \leqslant t_1 \\ a_2 t + b_2, & t \geqslant t_1 \end{cases}$ T_0: Room temperature For ASTM-E119 Standard fire: $a_1 = 78, a_2 = 1.8$ °C/min. $b_2 = 783.2$ °C $t_1 = 10$ m in.
α^2 (Thermal diffusivity of the section's material)	$\alpha^2 = \frac{k}{\rho c_p}$
$z_n, n = 1\ to\ 4$ (First four positive roots of the Bessel function, $J_0(z)$)	$z_1 = 2.405,\ z_2 = 5.520,\ z_3 = 8.654,\ z_4 = 11.792$

3.3. Verification of the heat transfer solution

The analytical approach described in the previous section was applied to a column selected from a series of fire tests conducted on CFDST columns by Imani et al. [16]. The selected specimen (referred to as Specimen S3 in that study) was a 3048 mm (10 foot) high CFDST column with outer and inner tube diameters of 203.2 and 127.0 mm (8 and 5 in.), respectively, and thicknesses of 2.8 mm (0.11 in.) for the outer, and 2.3 mm (0.09 in.) for the inner tube. The area between these tubes was filled with 60 MPa (8.8 ksi) concrete. The tubes were capped with steel plates at the top and bottom ends. A built up section (composed of steel plates and channels) was added to the bottom end of the specimen (to serve the needs of subsequent seismic testing). An additional built-up section (composed of steel plates and concrete infill) was added to the bottom end of the column for length extension before fitting inside the vertical fire furnace. Note that the mentioned built-up section was oriented in the plane of the furnace (it did not contribute to the out of plane bending).

The undamaged CFDST column was subjected to a constant axial load of 311.4 kN (70 kips) and a controlled air temperature inside the furnace following the ASTM E119 standard fire curve. Note that the mentioned CFDST column is referred to as "the specimen" in the rest of this paper. Since the time–temperature curve recorded on the surface of the outer tube of the specimen differed slightly from the standard ASTM E119 curve, a new bilinear function ($f(t)$) was fitted to the recorded curve, as follows:

$$f_{S_3}(t) = \begin{cases} 17.03t + 20, & t \leqslant 42.75\ \text{min}. \\ 4.27t + 565.49, & t \geqslant 42.75\ \text{min}. \end{cases} \quad (24)$$

Fig. 2c plots the recorded values of temperature versus the fitted bilinear function with first derivatives:

$$f'_{S_3}(t) = \begin{cases} a_1 = 17.03, & t \leqslant 42.75\ \text{min}. \\ a_2 = 4.27, & t \geqslant 42.75\ \text{min}. \end{cases} \quad (25)$$

Substituting Eqs. (24) and (25) into Eq. (23), the temperature distribution in the cross-section of the specimen can be calculated using the set of parameters: $r_o = 4$ in., $r_i = 2.5$ in., as given by Imani et al. [16] and α^2 (Eq. (4)) specified for concrete. Eurocode 4 general rules for structural fire design specify temperature independent values for the specific heat and thermal conductivity of concrete to be used in simplified calculation procedures. The specified constant values of 1000 J/kg °C for the specific heat and 1.6 W/m °C for the thermal conductivity of concrete were used here. Fig. 2d and e show the temperature dependent versus constant values for both of these parameters. Note that the specific heat parameter shows little variation as a function of temperature. Thermal conductivity, on the other hand, changes significantly at higher temperature levels. Therefore, using the recommended constant value consequently increases the rate of heat transfer through the concrete material, leading to slightly conservative predictions of the axial load capacity of the column at the end of the process. Recall that constant values for these parameters must be used here because the governing partial differential equation was solved with the assumption of a constant α. Assuming a density of 140 lb/in^3 (2242 kg/m^3) for concrete (normal weight), α^2 can be calculated as:

$$\alpha^2 = \frac{k}{\rho c_p} \cong 0.07\ \text{in}^2/\text{min}. \cong 7.13 \times 10^{-7}\ \text{m}^2/\text{s} \quad (26)$$

Available experimental data [16], along with results from finite element simulations of fire tests on CFDST columns were used to verify the accuracy of Eq. (23) in predicting temperature values in the inner parts of the column when the temperature of outer steel tube (as a function of time) is given as the input. Finite

element simulations paralleled the experiments by a sequentially coupled nonlinear thermal-stress analysis to study the effects of CFDST column's exposure to the Standard ASTM E119 fire. Analysis results from 3D models using material properties adopted from the Eurocode 4 general rules for structural fire design provided a reasonable comparison to experimental results.

Fig. 3a shows the variation of temperature through time for a point at mid-width of the concrete section, as obtained from test recordings [16], finite element simulations [21,22] and the analytical solution proposed for the heat transfer equation (Eq. (23)).

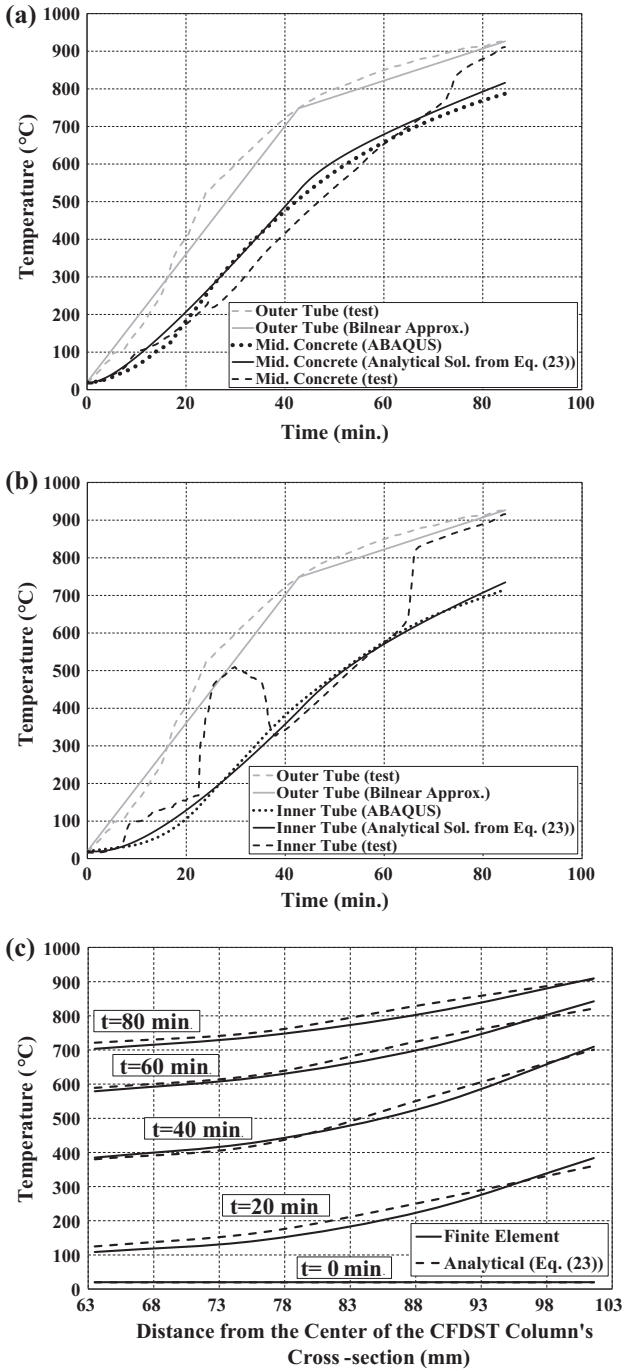

Fig. 3. Temperature distribution inside a CFDST column from the results of fire test for specimen S3 [16], finite element simulation [21,22] and the analytical solution (Eq. (23)): (a) time history at a point at mid-width of the concrete section; (b) time history at a point on the surface of inner steel tube; (c) variation of temperature through the thickness of the specimen.

Note that the analytical curves shown for the outer tube temperature are arbitrary (but accurate enough) bilinear representations of the recorded values that were used as inputs for the solution and are not part of the results. Having this input, Eq. (23) was used to calculate temperature values for points with $r_1 = 3.25$ in. (corresponding to a point at mid-width of concrete) and $r_2 = r_i = 2.5$ in. (corresponding to a point on the outer surface of the inner tube) as a function of time. The analytical solution is in good agreement with the experimental and numerical (FE analysis) results.

Note that, especially in the last 40 min of the fire, temperature values obtained from Eq. (23) are slightly higher than the ones from finite element analyses. This is contradictory to the fact that the bilinear approximation used for the temperature curve (which was applied as a boundary condition to the outer tube) had lower temperatures than the ones from the recorded data (also used in the finite element model). This discrepancy was caused by using a constant diffusivity parameter (α) for concrete in the analytical solution (Eq. (23)). Using the constant value based on Eurocode 4 leads to slightly conservative results (i.e. higher temperature values for a certain point at a certain time) as shown in Fig. 3a. The finite element results, on the other hand, were based on detailed 3D models of CFDST columns with nonlinear material models for steel and concrete that simulated the conduction and radiation mechanisms and accounted for temperature dependency of heat transfer parameters for each material [21,22].

Fig. 3b shows similar results (as in Fig. 3a) for a point on the surface of the inner tube of the same specimen. Results from the finite element heat transfer analysis and the analytical solution (Eq. (23)) are in good agreement. The test results, however, show significantly higher temperatures than those of the other two curves during certain periods of the fire test. The difference is attributed to sudden fluctuations of the recorded temperature possibly due to pressure built-ups and releases in the CFDST columns, an issue which was not accounted for in either of the finite element or analytical (Eq. (23)) approaches. Test results for inner tube temperature seem to be significantly higher than the predicted values, meaning the predictions can be unconservative. However, it should be noted that the predictions follow the general trend seen in the experiment, and the spikes in the inner tube temperature, which could not be captured in predictions, were more likely localized heat effects and did not have a significant impact on the column behavior. Results of the finite element simulations showed that the models were successful in predicting the overall behavior and fire resistance of CFDST columns [21,22].

To further investigate the accuracy of Eq. (23) in calculating the distribution of temperature in the cross-section of a CFDST column, temperature variation through the thickness of the concrete layer are plotted in Fig. 3c. A comparison with finite element analysis of the same specimen [21,22] for a number of points in time (i.e., $t = 0, t = 20, t = 40, t = 60$ and $t = 80$ min.) shows good agreement. Acceptable results of the simplified method supports the assumption of negligible radiation and convection effects inside the CFDST column.

4. Calculation of the axial load capacity of CFDST columns subjected to fire

4.1. Development of the analytical procedure

Given the temperature distribution through the cross-section of a CFDST column, its axial load capacity can be calculated using the modified material properties at a given time during exposure to the ASTM E119 (or any other defined) fire curve. Uniform temperature values for the outer steel tube with radius r_o (Fig. 1c) at time

t^* measured from the start of the outer tube's exposure to the bilinear fire curve, $f(t)$, is given by:

$$T_{ost,t^*} = f(t^*) \tag{27}$$

and the uniform temperature of the inner steel tube with radius r_i is given by:

$$T_{ist,t^*} = u(r_i, t^*) \text{ (using Eq. (23))} \tag{28}$$

The concrete section can be divided into n concentric layers with each layer having a uniform temperature distribution (Fig. 1c). This discretization can account for the non-uniform temperature distribution in the concrete section, with its accuracy dependent on the selected number of layers (i.e., a larger n leads to better accuracy). The uniform temperature for each layer is selected to be equal to the temperature of the point located on a circle going along the mid-width of the layer.

Uniform temperature values for concrete layer i (shown in Fig. 1c) at time t^* measured from the start of the outer tube's exposure to the fire curve, $f(t)$, is given by:

$$T_{cr_i,t^*} = u\left(\frac{(2n-1)(r_o - t_o - r_i)}{2n}, t^*\right) \text{ (using Eq. (23))} \tag{29}$$

where t_o is the thickness of the outer tube and n is the number of concrete layers.

According to the Eurocode general rules for structural fire design [4], the complete stress–strain relationship for steel at a given temperature can be constructed using four parameters: elastic modulus ($E_c(T)$), proportional limit stress ($f_p(T)$), effective yield stress ($f_y(T)$) and tensile strength ($f_u(T)$). The curve constructed using these parameters is shown in Fig. 4. Eurocode provides tabulated data for determining the four parameters at different temperatures. To simplify the calculation of these parameters at any given temperature, approximate fitted curves were developed in this study as follows:

The reduction factor for elastic modulus of steel, R_{E_s}, at temperature T is given by:

$$R_{E_s,T} = \frac{E_s(T)}{E_s} = \frac{1}{1 + \left(\frac{T}{523}\right)^4} - 0.04 \tag{30}$$

in which T is in °C and E_s is the elastic modulus at room temperature. Similarly for the yield stress, the reduction factor, R_{f_y}, is given by:

$$R_{f_y,T} = \frac{f_y(T)}{f_y} = \begin{cases} 1, & T \leqslant 400 \\ \frac{1.10}{1+\left(\frac{T}{572}\right)^{6.54}}, & T > 400 \end{cases} \tag{31}$$

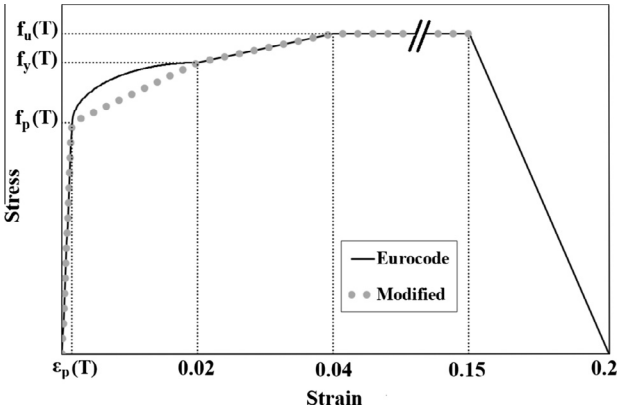

Fig. 4. Stress–strain curve of steel in uniaxial tension at temperature T (Eurocode curve compared with the simplified function (Eq. (42))).

in which T is in °C and f_y is the yield stress at room temperature. The reduction factor for the proportional limit stress, R_{f_p}, can be calculated as:

$$R_{f_p,T} = \frac{f_p(T)}{f_p} = \begin{cases} 1, & T \leqslant 100 \\ 1.27 - 2.71\times10^{-3}T + 1.71\times10^{-6}T^2 - 2.69\times10^{-10}T^3, & T > 100 \end{cases} \tag{32}$$

in which f_p is the proportional limit stress at room temperature. Note that $f_p = f_y$ for room temperature ($T = 20$ °C). Finally, the tensile stress of steel at temperature T is given as:

$$f_u(T) = \begin{cases} 1.25 f_y(T), & T \leqslant 400 \\ f_y(T), & T > 400 \end{cases} \tag{33}$$

Fig. 5 compares the tabulated data from Eurocode for the reduction factors mentioned above (R_{E_s}, R_{f_y} and R_{f_p}) with the proposed fitted functions. The functions are shown to be sufficiently accurate.

According to the Eurocode specifications for concrete at high temperatures, the ascending branch of the stress–strain curve for concrete in compression at temperature, T, can be constructed using two parameters, namely the compressive strength (f'_c) and the strain at maximum stress ($\varepsilon_{cu}(T)$). Note that after this point, the curve continues with a descending branch, down to a zero stress at the strain of $\varepsilon_{ce}(T)$.

A fitted function was also developed here for the reduction factor to adjust the maximum compressive strength of concrete at high temperatures, $R_{f'_c}$, based on the tabulated data provided in Eurocode 4. The resulting equation for $R_{f'_c}$ is given by:

$$R_{f'_c,T} = \frac{f'_c(T)}{f'_c} = \frac{1.12}{1 + \left(\frac{T}{597}\right)^{3.27}} - 0.13 \tag{34}$$

in which T is in °C and f'_c is the maximum compressive stress of concrete at room temperature. Using two additional fitted functions, $\varepsilon_{cu}(T)$ and $\varepsilon_{ce}(T)$ can be calculated as:

$$\varepsilon_{cu}(T) = \begin{cases} 1.75\times10^{-3} + 3.45\times10^{-5}T - 1.22\times10^{-7}T^2 + 2.14\times10^{-10}T^3, & x < 600 \\ 0.025, & x \geqslant 600 \end{cases} \tag{35}$$

$$\varepsilon_{ce}(T) = 1.99\times10^{-2} + 2.50\times10^{-5}T \tag{36}$$

Figs. 5d, e and f show plots of the values of $R_{f'_c,T}$, $\varepsilon_{cu}(T)$ and $\varepsilon_{ce}(T)$ extracted from tabulated data in Eurocode, along with the ones calculated using Eqs. (34)–(36). The fitted functions are shown to follow the Eurocode's specifications accurately.

Now that the stress at both steel and concrete sections can be calculated as a function of strain and temperature ($\sigma(\varepsilon, T)$), the total applied axial load on a CFDST column can be calculated as:

$$P_{axial}(\varepsilon, T) = A_{ost}\sigma_{ost}(\varepsilon, T) + A_{ist}\sigma_{sti}(\varepsilon, T) + \sum_{i=1}^{n} A_{cr_i}\sigma_{cr_i}(\varepsilon, T) \tag{37}$$

in which $A_{ost/ist/cr_i}$ refers to the area of the outer steel tube, inner steel tube, and ith concrete layer, respectively. Likewise, $\sigma_{ost/ist/cr_i}(\varepsilon, T)$ refers to the value of uniform stress in the same components as a function of strain and temperature, which can be calculated using the stress–strain relationships mentioned above. Note that the formula is written for a concrete region divided into n layers and assumes a compressive strain uniformly distributed over the cross-section. In each of the terms on the right hand side of Eq. (37), T refers to the temperature of one specific layer (inner tube,

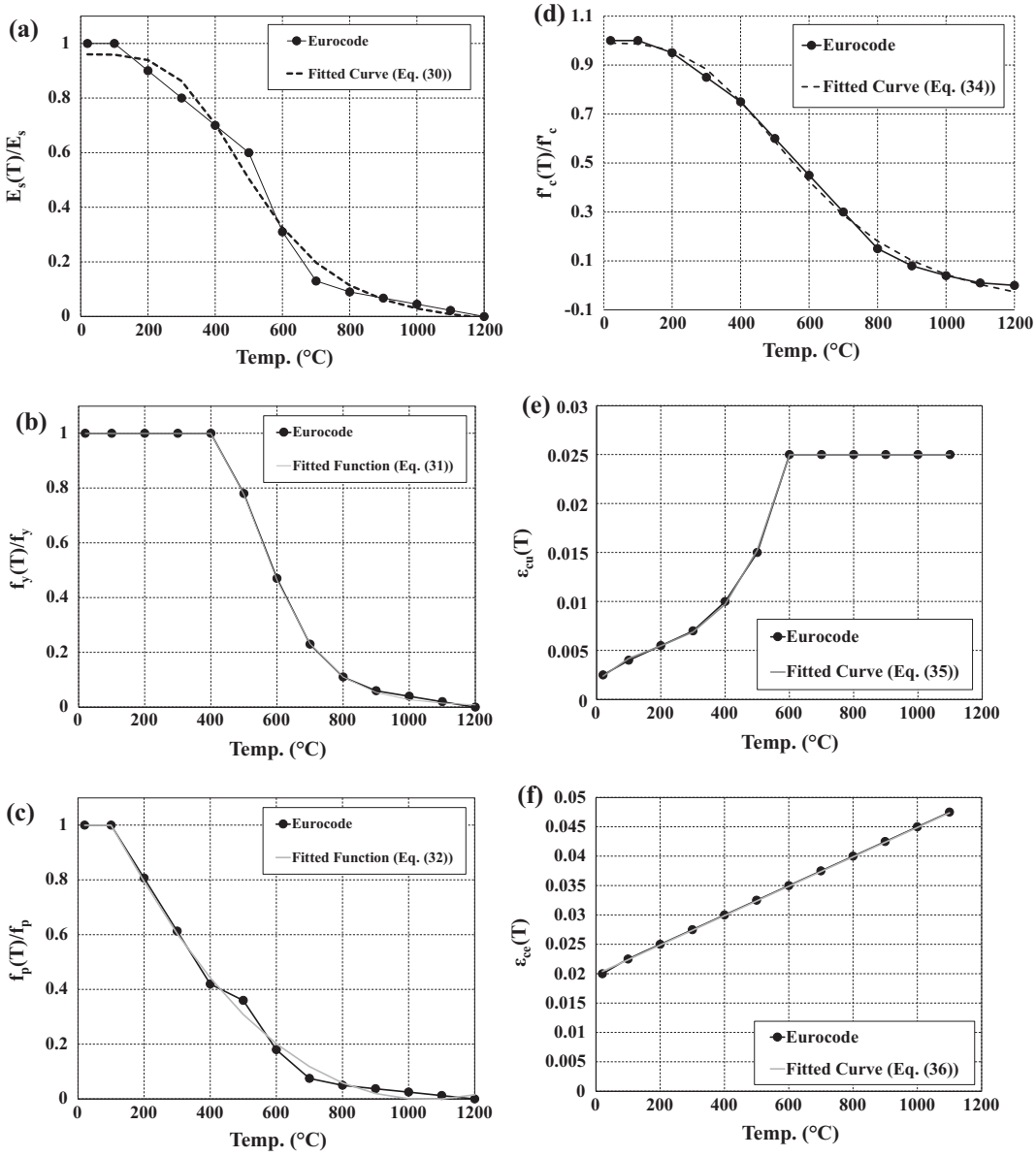

Fig. 5. Reduction factor for the structural properties of steel and concrete at high temperatures (tabulated data from Eurocode [4] vs. calculated values from the proposed fitted functions): for steel: (a) elastic modulus; (b) yield stress; (c) proportional limit stress; for concrete: (d) maximum compressive strength; (e) strain at maximum compressive stress; (f) strain at zero compressive stress (ultimate strain).

outer tube, or concrete) at a certain time (the *ost*, *ist* and cr_i indices for T have been removed for simplification). At a certain temperature, when going from zero to higher values of strain, $P_{axial}(\varepsilon, T)$ increases to its maximum value, attained when the steel and concrete layers reach a uniform stress distribution at their maximum strength values ($f_u(T)$ *and* $f'_c(T)$).

The critical buckling load as a function of strain and temperature, $P_{critical}(\varepsilon, T)$, can be written as:

$$P_{critical}(\varepsilon,T)=\frac{\pi^2}{(KL)^2}\left[I_{ost}E_{t_{ost}}(\varepsilon,T)+I_{ist}E_{t_{sti}}(\varepsilon,T)+\sum_{i=1}^{n}I_{cr_i}E_{t_{cr_i}}(\varepsilon,T)\right] \tag{38}$$

in which, $I_{ost/ist/cr_i}$ and $E_{t_{ost/ist/cr_i}}(\varepsilon, T)$ refer to the moment of inertia and tangent modulus values for the different sections, and KL is the effective length of the column. Note that the use of the tangent modulus in Eq. (38) allows for the calculation of the elastic and inelastic critical buckling loads as the materials go through increasing values of strain. At any given temperature level, the tangent moduli of steel and concrete decrease while going towards higher strain values. Therefore, Eq. (38) returns the maximum value for $P_{critical}(\varepsilon, T)$ at $(\varepsilon = 0)$ (calculated $P_{critical}(\varepsilon, T)$ remains constant or decreases as ε increases). According to the Eurocode specifications, the tangent modulus of steel heated to the temperature of T, can be calculated as:

$$E_{s_t}(\varepsilon,T)=\begin{cases}E_s(T), & \varepsilon<\varepsilon_p(T)\\ \frac{b(0.02-\varepsilon)}{a\sqrt{a^2-(0.02-\varepsilon)^2}}, & \varepsilon_p(T)<\varepsilon<0.02\\ \frac{f_u(T)-f_y(T)}{0.02}, & 0.02<\varepsilon<0.04\\ 0, & 0.04<\varepsilon<0.15\end{cases} \tag{39}$$

Note that Eq. (39) is given for strains up to the start of the descending branch of the uniaxial tensile behavior and must be used separately for the inner and outer steel tubes, as they would be at different temperature levels. Similarly for concrete, the tangent modulus for strains up to the limit of compressive strength can be calculated as:

$$E_{c_t}(\varepsilon,T)=f_c(T)\left[\frac{3}{2+\left(\frac{\varepsilon}{\varepsilon_{cu}(T)}\right)^3}-\frac{\frac{9}{\varepsilon_{cu}(T)}\left(\frac{\varepsilon}{\varepsilon_{cu}(T)}\right)^3}{\left[2+\left(\frac{\varepsilon}{\varepsilon_{cu}(T)}\right)^3\right]^2}\right] \tag{40}$$

Eq. (40) can be used separately for each of the $n$layers of concrete at their respective calculated uniform temperature. Fig. 6a shows generic plots for the $P_{axial}(\varepsilon,T)$ and $P_{critical}(\varepsilon,T)$ functions for a fixed (current) T for each of the steel and concrete layers and a varying ε. Finally, the axial load capacity of the column after a certain duration of exposure to a given fire curve can be determined from the intersection of the two functions $P_{axial}(\varepsilon,T)$ and $P_{critical}(\varepsilon,T)$ (Eqs. (37) and (38)), as shown in Fig. 6a. Defining ε_{int} as the strain value of the intersection point gives:

$$P_{axial\ Capacity}(T)=P_{axial}(\varepsilon_{int},T)=P_{critical}(\varepsilon_{int},T) \tag{41}$$

Assuming a uniform temperature distribution in each of the concrete sections, the inner tube, and the outer tube, Eq. (41) can be solved by incrementally increasing the strain value up to the point when the two load functions ($P_{axial}(\varepsilon,T)$ and $P_{critical}(\varepsilon,T)$) return the same load, which is then the axial capacity of the column. This part of the procedure (i.e., solving Eq. (41) by incrementally increasing the strain value) is similar to what is presented in the simple calculation method described in Annex H of the Eurocode 4 general rules for structural fire design. Alternatively, the equation can be solved graphically by plotting the two curves as functions of strain and finding their intersecting point.

A more simplified procedure was developed to provide an acceptable approximation of the axial load capacity of CFDST columns by calculating the values of $P_{axial}(\varepsilon,T)$ and $P_{critical}(\varepsilon,T)$ at a few selected key points. The procedure is presented in the following section.

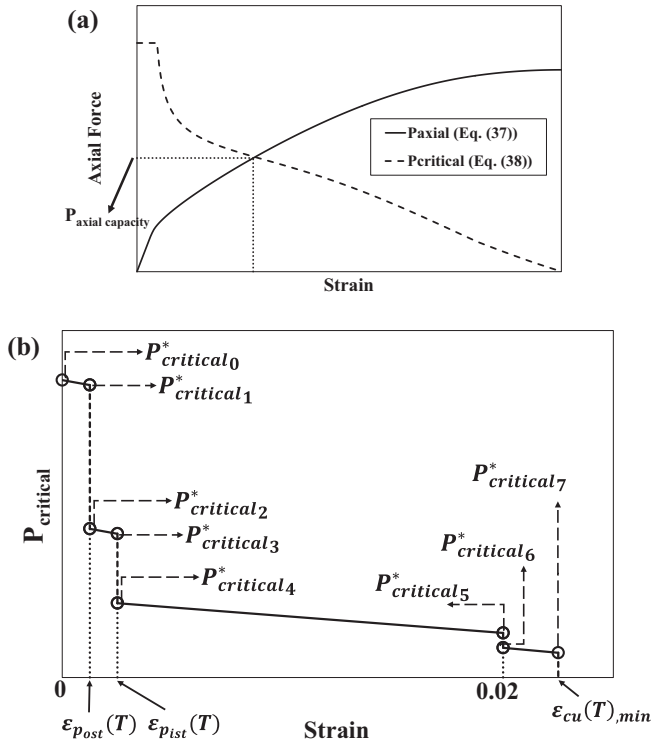

Fig. 6. Generic plots of the $P_{axial}(\varepsilon,T)$ and $P_{critical}(\varepsilon,T)$ functions for a fixed T and varying ε: (a) the intersection of $P_{axial}(\varepsilon,T)$ and $P_{critical}(\varepsilon,T)$; (b) simplified $P^*_{critical}(\varepsilon,T)$ (Eq. (47)).

4.2. Simplified step by step procedure to calculate the axial load capacity of CFDST columns under fire

To reduce the complexity of the analytical approach described above for calculating the axial load capacity of CFDST columns subjected to fire, an alternative set of simplified equations were selected to calculate the uniform stress and tangent modulus to be used in the different parts of the cross-sections, as functions of strain and temperature. For steel, as shown in Fig. 4, the elliptical part of the Eurocode stress–strain curve (for strains in the range $\varepsilon_p<\varepsilon<0.02$), which has a varying tangent modulus as specified in Eq. (39), was replaced by a multi-linear curve, turning the reference curve into four linear segments. The new stress–strain relationship for different strain ranges with their corresponding tangent modulus is given as:

$$\sigma^*_{steel}(\varepsilon,T)=\begin{cases}E_{s_1}(T)\varepsilon, & \varepsilon<\varepsilon_p(T)\\ f_p(T)+E_{s_2}(\varepsilon-\varepsilon_p(T)), & \varepsilon_p(T)<\varepsilon<0.02\\ f_y(T)+E_{s_3}(\varepsilon-0.02), & 0.02<\varepsilon<0.04\\ f_u(t), & 0.04<\varepsilon<0.15\end{cases} \tag{42}$$

in which $\sigma^*_{steel}(\varepsilon,T)$ is the simplified function for the stress–strain relationship of steel at temperature T. Note that $E_{s_1},E_{s_2},E_{s_3},E_{s_4}$ refer to the tangent modulus of steel over different strain ranges and are given as:

$$E^*_{s_t}(\varepsilon,T)=\begin{cases}E_{s_1}(T)=E_s(T), & \varepsilon<\varepsilon_p(T)\\ E_{s_2}(T)=\frac{f_y(T)-f_p(T)}{0.02-\varepsilon_p(T)}, & \varepsilon_p(T)<\varepsilon<0.02\\ E_{s_3}=\frac{f_u(T)-f_y(T)}{0.02}, & 0.02<\varepsilon<0.04\\ E_{s_4}=0, & 0.04<\varepsilon<0.15\end{cases} \tag{43}$$

Similarly for concrete, since the stress–strain relationship given in the Eurocode leads to a complicated nonlinear equation for the tangent modulus (Eq. (40)), Hognestad's equation [23], which is a polynomial of degree two, was used to express the stress–strain relationship for concrete as follows:

$$\sigma^*_{concrete}(\varepsilon,T)=f'_c(T)\left[\frac{2\varepsilon}{\varepsilon_{cu}(T)}-\left(\frac{\varepsilon}{\varepsilon_{cu}(T)}\right)^2\right] \tag{44}$$

in which $f'_c(T)$ and $\varepsilon_{cu}(T)$ are calculated based on the Eurocode specifications (using the fitted functions presented above in Eqs. (34) and (35)). Note that Eq. (44) gives the stress–strain relationship up to the point of maximum compressive stress, $f'_c(T)$, which occurs at the strain of $\varepsilon_{cu}(T)$ for concrete at a given temperature, T. Taking the first derivative of Eq. (44) with respect to ε, the tangent modulus for concrete can then be calculated as:

$$E^*_{c_t}(\varepsilon,T)=\frac{2f'_c(T)}{\varepsilon_{cu}(T)}\left[1-\frac{\varepsilon}{\varepsilon_{cu}(T)}\right] \tag{45}$$

which is a simple linear equation in terms of ε. Note that the '*' used in the equations above is used to distinguish the new simple equations from the previously presented Eurocode equations for the same parameters. Using the new set of equations for the stress and tangent modulus calculation, Eqs. (37) and (38) are rewritten as:

$$P^*_{axial}(\varepsilon,T)=A_{ost}\sigma^*_{ost}(\varepsilon,T)+A_{ist}\sigma^*_{sti}(\varepsilon,T)+\sum_{i=1}^{n}A_{cr_i}\sigma^*_{cr_i}(\varepsilon,T) \tag{46}$$

$$P^*_{critical}(\varepsilon,T)=\frac{\pi^2}{(KL)^2}\left[I_{ost}E^*_{t_{ost}}(\varepsilon,T)+I_{ist}E^*_{t_{sti}}(\varepsilon,T)+\sum_{i=1}^{n}I_{cr_i}E^*_{t_{cr_i}}(\varepsilon,T)\right] \tag{47}$$

Now redrawing the curve for the critical buckling load from Fig. 6a, this time with more details, according to the changes of the tangent moduli of steel and concrete over different strain ranges, a number of discontinuity points occur in the curve as

shown in Fig. 6b. The discontinuities are caused by sudden changes in the tangent modulus of steel when the strain in each of the inner or outer tubes gets past the limits of $\varepsilon_p(T)$ (which is different for the outer and inner steel tubes) and 0.02. Note that changes in the tangent modulus of concrete do not create discontinuities because it is defined as the first derivative of a continuous function.

Considering the possible range of values for $\varepsilon_{cu}(T)$ according to the Eurocode specifications ($0.0025 \leqslant \varepsilon_{cu} \leqslant 0.025$), the strain limits $\varepsilon_1, \varepsilon_2, \varepsilon_3$ and ε_4 can be determined as follows:

$$\begin{aligned}
&\varepsilon_1 = \varepsilon_{0p_{ost}}(T)\\
&\varepsilon_2 = \varepsilon_{p_{ist}}(T)\\
&\varepsilon_3 = min\{0.02, min_{i=1-n}\{\varepsilon_{cu_i}(T)\}\}\\
&\varepsilon_4 = min_{i=1-n}\{\varepsilon_{cu_i}(T)\} \text{ (applicable only if } \varepsilon_3 = 0.02)
\end{aligned} \tag{48}$$

The first strain limit (i.e., ε_1), refers to the point when the outer steel tube reaches the end of its proportional limit according to Fig. 4 (ε_p). Note that the outer steel tube will always reach ε_p sooner than the inner tube because the outer steel tube is at a higher temperature level and, according to Eurocode specifications for steel material, $\varepsilon_p(T)$ decreases as temperature increases. Therefore, $\varepsilon_{p_{ost}} < \varepsilon_{p_{ist}}$. The second discontinuity in the $P^*_{critical}$ curve occurs when the strain value of the cross-section reaches $\varepsilon_{p_{ist}}$, which is referred to as the ε_2 limit. Two different scenarios must be considered for determination of ε_3. This limit is defined as the smaller of 0.02, i.e., when steel starts the hardening branch (shown in Fig. 4) and the smallest strain value that gets one of the concrete layers to the maximum stress point (ε_{cu}).

Note that according to Eq. (48), the ε_4 limit is only needed if $\varepsilon_3 = 0.02 < min_{i=1-n}\{\varepsilon_{cu_i}(T)\}$. In other words, the curve in Fig. 6b needs to be continued up to the point when the uniform strain in the section reaches to the limit of $\varepsilon_{cu}(T)$ for one of the concrete layers, which will be the limit of $\varepsilon = min_{i=1-n}\{\varepsilon_{cu_i}(T)\}$. The behavior of concrete in compression enters the descending branch at this point and Eq. (45) can no longer be used for the calculation of the tangent modulus. However, when the strain level in the section reaches this limit, total critical buckling load has dropped more than needed to create an intersection with the applied axial load, $P^*_{axial}(\varepsilon, T)$, or if not, the force level is low enough to consider the column to have no axial resistance at that temperature level. This makes the rest of the $P^*_{critical}(\varepsilon, T)$ curve, irrelevant (because the $P^*_{axial}(\varepsilon, T)$ curve will start to descend after this point). Note that the strain limits in Fig. 6b are based on the assumption that $min_{i=1-n}\{\varepsilon_{cu_i}(T)\} > 0.02$.

Note that $\varepsilon_{p_{ost}}(T)$ will always be lower than $\varepsilon_{p_{ist}}(T)$ because the outer steel tube is at a higher temperature level (according to Eurocode specifications, for a certain steel, $\varepsilon_p(T)$ decreases as temperature increases). According to the strain limits defined in Eq. (48), the tangent moduli for the inner and outer tubes at the temperatures of T_{ost} and T_{ist} are given as:

$$E_{ost_t}(T_{ost}), E_{ist_t}(T_{ist}) = \begin{cases} E_{ost_1}(T), E_{ist_1}(T) & \varepsilon < \varepsilon_1 \\ E_{ost_2}(T), E_{ist_1}(T) & \varepsilon_1 < \varepsilon < \varepsilon_2 \\ E_{ost_2}(T), E_{ist_2}(T) & \varepsilon_2 < \varepsilon < 0.02 \\ E_{ost_3}(T), E_{ist_3}(T) & 0.02 < \varepsilon < 0.04 \end{cases} \tag{49}$$

in which $E_{ost/ist_{1-3}}$ are calculated using Eq. (43). Note that the location of the strain limits ε_3 and ε_4 with respect to the 0.02 and 0.04 limits must be determined specifically for a given problem. At this point, the intersection of the two curves defined by the functions, $P^*_{axial}(\varepsilon, T)$ and $P^*_{critical}(\varepsilon, T)$ (Eq. (46)), which is equal to the axial load capacity of the CFDST column after being exposed to the first t minutes of a given fire curve, $f(t)$, can be determined by following these steps:

Step1. Using the analytical solution derived for the heat transfer problem (Eq. (23)), determine the uniform temperature values for the outer steel tube, inner steel tube and all of the $n$concentric concrete layers at time t after the start of the CFDST column's exposure to the given fire curve, $f(t)$.

Step2. Determine $\varepsilon_1, \varepsilon_2, \varepsilon_3$ and ε_4 (if applicable) for the column using Eq. (48).

Step3. Calculate the critical buckling load, using the tangent moduli of different steel and concrete regions, for the strain values shown with dots in Fig. 7a, if $\varepsilon_3 = min_{i=1-n}\{\varepsilon_{cu_i}(T)\}$, or Fig. 7b, if $\varepsilon_3 = 0.02, \varepsilon_4 = min_{i=1-n}\{\varepsilon_{cu_i}(T)\}$. Note that these critical buckling load values are referred to as $P^*_{critical_0}, P^*_{critical_1}, \ldots, P^*_{critical_5}$ for the first case and $P^*_{critical_0}, P^*_{critical_1}, \ldots, P^*_{critical_7}$ for the second case, as shown in Fig. 6b. Recall that the sudden drops (discontinuities) occur due to the sudden changes in the tangent modulus of steel as the strain value jumps from one of the strain ranges defined in Eq. (48) to the other. The infinitesimal value ϵ is used to distinguish between the tangent modulus when the strain is just below or just above one of the strain ranges defined in Eq. (48). The slight gradual decreases seen between any two discontinuity points in Fig. 6b are caused by the gradual reduction of the concrete tangent modulus as the curve goes to higher strains.

Step4. Assuming $P^*_{axial_i} = P^*_{axial}(\varepsilon_i, T)$ that can be calculated using Eq. (46) for the strain values $\varepsilon_0 = 0, \varepsilon_2, \varepsilon_3$ and ε_4 (given by Eq. (48)), axial load capacity of the column can be determined through the simple iterative process defined in Eq. (50). Knowing that $P^*_{axial_0} = 0$ and starting from $i = 1$:

$$P_{axial\ capacity} = \begin{cases} \dfrac{P^*_{critical_{2i-2}} P^*_{axial_i} - P^*_{critical_{2i-1}} P^*_{axial_{i-1}}}{\left(P^*_{axial_i} - P^*_{axial_{i-1}}\right) - \left(P^*_{critical_{2i-1}} - P^*_{critical_{2i-2}}\right)}, & P^*_{critical_{2i-1}} < P^*_{axial_i} \\ P^*_{axial_i}, & P^*_{critical_{2i}} \leqslant P^*_{axial_i} \leqslant P^*_{critical_{2i-1}} \\ Redo\ the\ process\ for\ i = i+1, & P^*_{axial_i} < P^*_{critical_{2i}} \end{cases} \tag{50}$$

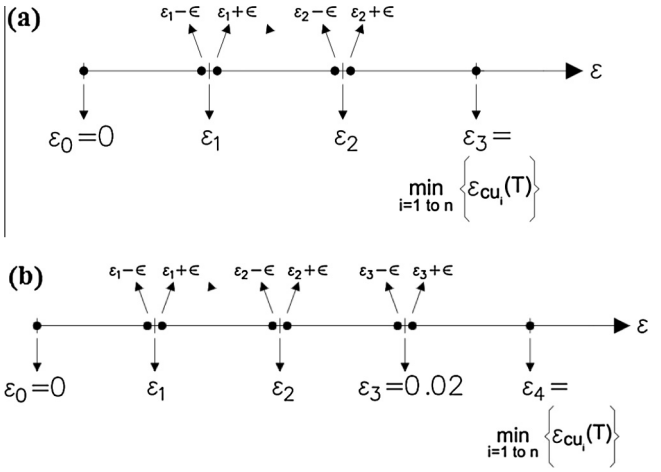

Fig. 7. Strain values needed for the calculation of $P^*_{critical_0}, \ldots, P^*_{critical_n}$: (a) cases with $\varepsilon_3 = min_{i=1-n}\{\varepsilon_{cu_i}(T)\}$ ($n = 5$); (b) cases with $\varepsilon_3 = 0.02, \varepsilon_4 = min_{i=1-n}\{\varepsilon_{cu_i}(T)\}$ ($n = 7$).

in which $P^*_{critical_i}$'s come from the calculation in step 3 and i_{max} is equal to 4 when the strain limit of ε_4 is defined according to Eq. (48), and to 3 otherwise.

Fig. 8 visually explains the logic used in the definition of Eq. (50). For a given i (which varies between 1 to 4 as explained before), three cases are possible with respect to $P^*_{axial_i}$. First case is when $P^*_{axial_i} > P^*_{critical_{2i-1}}$. This condition, as shown in Fig. 8a, ensures that an intersection will occur between the P^*_{axial} and $P^*_{critical}$ curves. Since determining the exact intersection is challenging, a straight line is defined using the points $P^*_{axial_i}$ and $P^*_{axial_{i-1}}$ and its intersection with the linear portion of the $P^*_{critical}$ curve is selected to be the axial load capacity of the column (i.e., $P^*_{axial\ capacity}$). First line of Eq. (50) calculates the axial load capacity for this case. Note that the equation provides a slightly conservative result compared to the exact solution (lower capacity).

The second case occurs when $P^*_{critical_{2i}} \leqslant P^*_{axial_i} \leqslant P^*_{critical_{2i-1}}$. In this case, as shown in Fig. 8b, the P^*_{axial} curve crosses the $P^*_{critical}$ curve when it drops due to a sudden change in elastic modulus of steel. In this configuration, the intersection occurs right at the point of $P^*_{axial_i}$. If $P^*_{axial_i} \leqslant P^*_{critical_{2i}}$ (the third case), no intersection can be found between the P^*_{axial} and $P^*_{critical}$ curves and new points on both curves need to be calculated ($i = i + 1$). Note that Fig. 8 (and similarly Figs. 4 and 6) show generic plots of curves which are used in the paper to explain their general trend and properties and explain the solution. These plots are not a solution for a specific case and do not have numerical values.

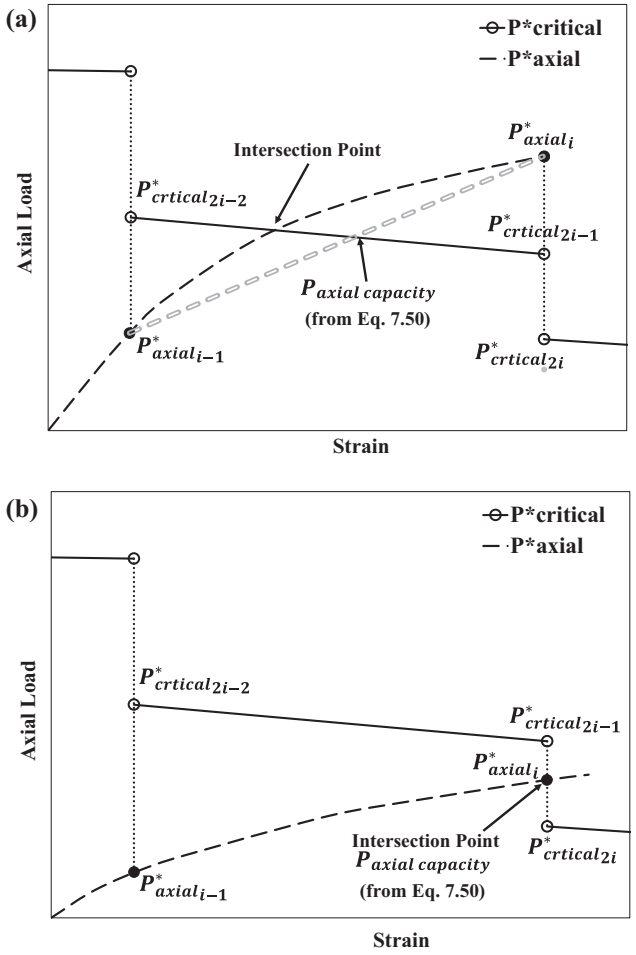

Fig. 8. Graphical explanation for calculating the axial load capacity using Eq. (50): (a) cases with $P^*_{critical_{2i-1}} < P^*_{axial_i}$; (b) cases with $P^*_{critical_{2i}} \leqslant P^*_{axial_i} \leqslant P^*_{critical_{2i-1}}$.

4.3. Verification of the analytical approach to calculate axial load capacity of CFDST columns under fire

The analytical approach described in Section 4.1 for calculating the axial load capacity of CFDST columns subjected to fire was applied to the same tested column from Imani et al. [16] that was used in Section 3.3 for the verification of the heat transfer solution. Knowing the temperature distribution in the cross-section of the specimen, which was calculated and verified using the solution described in Section 3, axial load capacity of the specimen can be calculated using Eq. (41), which equates two load curves that are determined using the stress distribution in different sections at certain temperature and strain levels, and the current critical buckling load of the column calculated according to the tangent modulus of different sections at certain temperatures. A simple MATLAB code was developed to generate the mentioned load curves and solve for the equation to determine the axial load capacity of any given CFDST column subjected to the first t minutes of a predetermined fire curve. Results from this MATLAB code for the mentioned specimen are presented later in this paper.

In addition to applying the procedure described in Section 4.1, the axial load capacity of the specimen subjected to the ASTM E119 fire curve was also determined using the simplified step by step procedure presented in Section 4.2 for verification.

According to the test results [16], the CFDST specimen had a fire resisting time of about 65 min under a constant axial load of 311.4 kN (70 kips). In a separate study, Imani et al. simulated the complete thermal-stress process using the finite element method, predicting a similar fire resisting time for the numerical model of the specimen [21,22]. To verify of the proposed analytical method described in Section 4.1, the axial load capacity of the CFDST specimen was calculated after 50, 65 and 80 min from the start of the outer tube's exposure to the bilinear fire curve defined by Eq. (24) (which follows the outer tube's recorded temperature curve from the test).

To assess the sensitivity of the assumed number of concrete layers, the procedure was conducted for two cases, namely $n = 2$ and $n = 3$. Using Eqs. (27)–(29), the uniform temperature values for the sections of inner and outer tubes, and the selected number of concrete layers, along with their corresponding temperature modified material properties were calculated for use in Eqs. (37) and (38). These parameters are presented in Table 2 with initial values for material properties at room temperature taken from the experimental study.

According to the study by Imani et al., the specimen was tested with fixed and semi-rigid connections at its top and bottom ends, respectively. Due to the lack of information about the properties of the semi-rigid connection at the bottom end, two different cases, with fixed and pinned connections at the base, were considered in the axial load capacity calculations. Fig. 9a and b show the buckling deformation of the column under the two mentioned configurations. Note that the bottom portion of the column, consisting of a built-up section (steel box filled with concrete) added to accommodate the cyclic test setup requirements, was assumed as a rigid segment with a total length of 355.6 mm. The remaining CFDST column height was 2692 mm.

For the fixed–fixed configuration (Fig. 9a), the corresponding effective length for use in Eq. (38) was calculated as $KL = 1346$ mm ($K = 0.5$), with $L = 2692$ mm. The critical buckling load for the fixed-pinned conditions needs to be calculated as a special case because the rigid part is engaged in the buckling deformation. Assuming $w(x)$ is the deflected shape of the column with x

Table 2
Uniform temperature and material properties calculated for different parts of the cross-section of the tested specimen after 50, 65 and 80 min. of exposure to the ASTM E119 fire.

	Steel regions	Outer tube	Inner tube	Concrete regions	$n=2$		$n=3$		
					1	2	1	2	3
Conditions	Outer radius (mm)	101.6	63.5	Outer radius (mm)	98.8	81.0	98.8	87.1	75.4
	Thickness (mm)	2.8	2.3	Thickness (mm)	17.8	17.8	11.7	11.7	11.7
Room temperature	E_s (MPa)	200,000	200,000	E_c (MPa)	38,696	38,696	38,696	38,696	38,696
	f_p (MPa)	345	303	f'_c (MPa)	66.9	66.9	66.9	66.9	66.9
	f_y (MPa)	345	303	ε_{cu}	0.0025	0.0025	0.0025	0.0025	0.0025
	f_u (MPa)	400	365	ε_{ce}	0.0200	0.0200	0.0200	0.0200	0.0200
After 50 min. of fire exposure	Temp. (°C)	778.9	440.1	Temp. (°C)	513.5	681.0	488.2	594.3	710.5
	$E_s(T)$ (MPa)	25,763	125,147	$f'_c(T)$ (MPa)	38	21	41	29	18
	$f_p(T)$ (MPa)	24.1	117	$\varepsilon_{cu}(T)$	0.0164	0.0250	0.0145	0.0242	0.0250
	$f_y(T)$ (MPa)	44.4	283	$\varepsilon_{ce}(T)$	0.0353	0.0403	0.0345	0.0377	0.0412
	$f_u(T)$ (MPa)	44.4	283	–	–	–	–	–	–
After 65 min. of fire exposure	Temp. (°C)	843.0	573.8	Temp. (°C)	634.1	767.0	613.5	698.8	790.0
	$E_s(T)$ (MPa)	17,793	73,655	$f'_c(T)$ (MPa)	25	14	27	19	13
	$f_p(T)$ (MPa)	13.9	69	$\varepsilon_{cu}(T)$	0.0250	0.0250	0.0250	0.0250	0.0250
	$f_y(T)$ (MPa)	27.8	165	$\varepsilon_{ce}(T)$	0.0389	0.0429	0.0383	0.0409	0.0436
	$f_u(T)$ (MPa)	27.8	165	–	–	–	–	–	–
After 80 min. of fire exposure	Temp. (°C)	907.1	678.6	Temp. (°C)	729.1	841.7	711.9	783.7	861.5
	$E_s(T)$ (MPa)	11,899	44,156	$f'_c(T)$ (MPa)	17	10	18	13	9
	$f_p(T)$ (MPa)	6.5	41	$\varepsilon_{cu}(T)$	0.0250	0.0250	0.0250	0.0250	0.0250
	$f_y(T)$ (MPa)	17.7	82	$\varepsilon_{ce}(T)$	0.0418	0.0452	0.0413	0.0434	0.0457
	$f_u(T)$ (MPa)	17.7	82	–	–	–	–	–	–

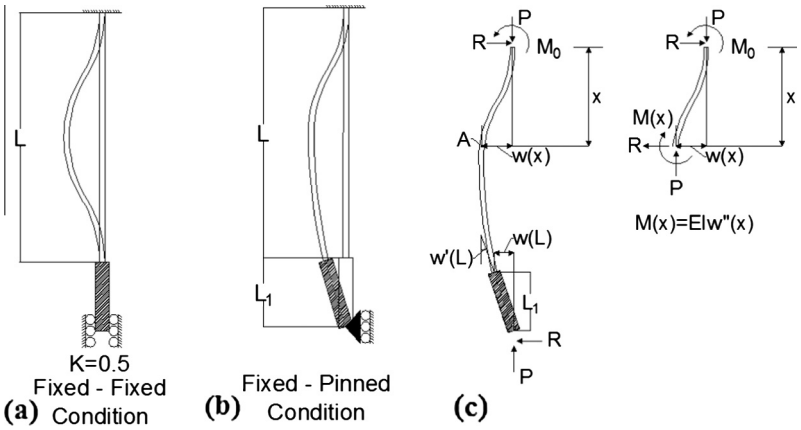

Fig. 9. Buckling deformation of the CFDST column with the rigid part at the bottom end subjected to different boundary conditions: (a) fixed–fixed configuration; (b) fixed-pinned configuration; (c) free body diagrams for the fixed-pinned configuration

measured from the top end of the column as shown in Fig. 9c, the governing differential equation and the appropriate boundary conditions can be written as [24]:

$$EIw''(x)+Pw(x)+R(x-L-L_1),\quad 0\leqslant x\leqslant L$$
$$B.C.'s:\begin{cases}(1)\quad w(0)=0\\(2)\quad w'(0)=0\\(3)\quad w(L)=L_1w'(L)\end{cases}\tag{51}$$

Eq. (51) is derived by satisfying the moment equilibrium at point A at a distance x. The general solution for the governing differential equation can be written as:

$$w(x)=a_1\sin(\mu x)+a_2\cos(\mu x)-\frac{R}{P}(x-L-L_1)\tag{52}$$

in which $\mu=\sqrt{P/EI}$ and the term $\left(-\frac{R}{P}(x-L-L_1)\right)$ is the particular solution (R is the support reaction at the pinned end). Satisfying the first and second boundary conditions gives:

$$a_1=\frac{R}{P\mu}\tag{53}$$
$$a_2=-\frac{R(L+L_1)}{P}\tag{54}$$

Substituting Eqs. (53) and (54) in Eq. (52) gives:

$$w(x)=\frac{R}{P\mu}\sin(\mu x)-\frac{R(L+L_1)}{P}\cos(\mu x)-\frac{R}{P}(x-L-L_1)\tag{55}$$

Applying the third boundary condition to Eq. (55), results in:

$$(L+2L_1)\cos(\mu L)+\left(L_1\mu(L+L_1)-\frac{1}{\mu}\right)\sin(\mu L)-2L_1=0\tag{56}$$

which must be solved for roots of μ, to obtain the critical buckling load values for different buckling modes ($P_{critical}=\mu^2EI$). If the rigid section length $L_1=0$, Eq. (56) reduces to $\tan(\mu L)=\mu L$, which has the smallest root of $\mu=4.493/L$ and leads to the familiar critical buckling load of $P_{critical}=20.19EI/L^2$ (equivalent to $K\cong 0.7$ for $P_{critical}=\pi^2EI/(KL)^2$).

Setting $L = 2692$ mm and $L_1 = 406.4$ mm, Eq. (56) was numerically solved to obtain the smallest root of $\mu \cong 0.05$. The corresponding critical buckling load is $P_{critical} = 2.5 \times 10^{-3} EI$. For $L = 2692$ mm, this is equivalent to taking $K = 0.593$ in the formula $P_{critical} = \pi^2 EI/(KL)^2$.

To determine the axial load capacity of the specimen, P_{axial} and $P_{critical}$ (defined in Eqs. (37) and (38)) were calculated for different strain values and plotted in Fig. 10 for the four cases considered (fixed–fixed and fixed-pinned, each with 2 and 3 concrete layers) after 65 min. of exposure to the ASTM E119 fire. Note that the plots were derived from the results of the MATLAB code written for the procedure that used the varying tangent moduli of steel and concrete (Eqs. (39) and (40)) for the calculation of $P_{critical}$ at different strain values.

Fig. 10 shows that the case with three concrete layers gives the same results as using two concrete layers (the results have converged with respect to the number of concrete layers for the specific problem in hand). The axial load capacity values calculated by solving Eq. (41) for different cases (namely, the specimen subjected to the first 50, 65 and 80 min of the standard ASTM E119 fire curve) are summarized in Table 3. Note that for 65 min of fire exposure, the cases with fixed–fixed and fixed-pinned end conditions have axial load capacity of 375.4 kN (84.1 kips) and 304.3 kN (68.4 kips), respectively. Considering that the column buckled under a load of 311.4 kN (70 kips) during the fire test, it was inferred that the end conditions were closer to the fixed-pinned case rather than the fixed–fixed one.

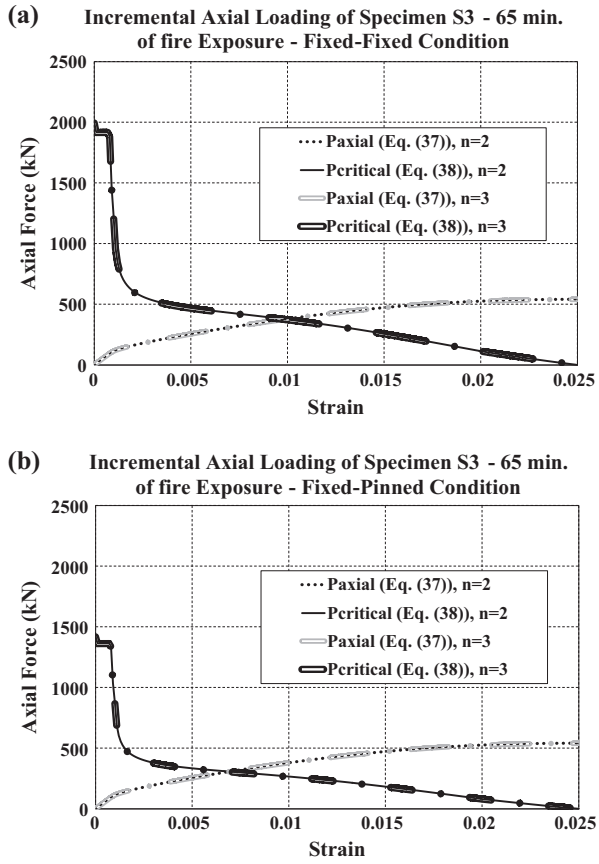

Fig. 10. P_{axial} and $P_{critical}$ functions plotted for Specimen S3 after 65 min of exposure to the ASTM E119 standard fire curve assuming: (a) fixed–fixed and (b) fixed-pinned end conditions for cases with different number of defined concrete layers ($\boldsymbol{n = 2}$ and $\boldsymbol{n = 3}$).

Table 3
Axial load capacity calculated for the tested specimen using the Analytical Approach (Eq. (41)) compared with finite element analysis [21,22] and test [16] results for different cases (force unit: kN).

Calculation method		Analytical Eq. (41)				Finite element analysis	Test results
End conditions		Fixed–fixed		Fixed-pinned		Fixed-pinned	Fixed-semi fixed
No. of concrete layers		$n = 2$	$n = 3$	$n = 2$	$n = 3$	–	–
Exposure time (min.)	50	638.1	623.9	538.5	526.9	582.1	–
	65	374.2	376.9	306.6	304.4	307.1	311.5
	80	240.3	238.5	196.2	194.5	218.1	–

Results for the 50, 65 and 80 min of fire exposure time were also verified with the buckling forces calculated for the specimen in using finite element analysis with ABAQUS in a separate study by Imani et al. [21]. From the results presented in Table 3, it is inferred that the results from applying the analytical approach to the case with the fixed-pinned end conditions are again reasonably close to the finite element analysis results, which were built with the assumption of fixed-pinned end conditions, and slightly conservative due to the assumptions made in the heat transfer part of the solution. Marginal differences between the results from the $n = 2$ and $n = 3$ cases confirm the convergence of the solution. Note that even though the $n = 2$ case coincidentally provided a closer estimate of the experimental value in this specific problem, the general solution strategy is to increase the number of levels as needed to achieve convergence.

As the last part of the verifications process, the simplified step by step approach described in Section 4.2 was applied to the specimen to calculate the axial load capacity after 65 min of exposure to the standard ASTM E119 fire curve. Since the first step of the process (the heat transfer solution) was already completed in the previous verification analysis (Section 3.3), the procedure started with the second step, which requires the calculation of the strain limits $\varepsilon_1, \varepsilon_2, \varepsilon_3, \varepsilon_4$ (if applicable) using Eq. (48). Using the information provided in Table 2, after 65 min of fire exposure time, the mentioned strain limits are calculated as:

$$\varepsilon_1 = \varepsilon_{p_{ost}}(T_{ost\,@\,65min.}) = \frac{f_{p_{ost}}(T_{ost\,@\,65min.})}{E_{s_{ost}}(T_{ost\,@\,65min.})} = \frac{2.01}{2581} = 7.79 \times 10^{-4}$$

$$\varepsilon_2 = \varepsilon_{p_{ist}}(T_{ist\,@\,65min.}) = \frac{f_{p_{ist}}(T_{ist\,@\,65min.})}{E_{s_{ist}}(T_{ist\,@\,65min.})} = \frac{9.97}{10684} = 9.33 \times 10^{-4}$$

$$\varepsilon_3 = min\{0.02, min_{i=1-n}\{\varepsilon_{cu_i}(T_{cr_i\,@\,65min.})\}\} = min\{0.02, 0.025\} = 0.02$$

$$\varepsilon_4 = min_{i=1-n}\{\varepsilon_{cu_i}(T_{cr_i\,@\,65min.})\} = 0.025 \qquad (57)$$

The next step is dedicated to the calculation of the $P^*_{critical_i}$'s for $i = 1 to 4$ using Eq. (47). These are the critical buckling loads at different strain levels, which are calculated using the tangent moduli of steel and concrete sections as explained in Section 4.2. The load values were calculated for the specimen after 65 min of exposure to the ASTM E119 fire and are reported in Table 4.

Using the load values summarized in Table 4, the axial load capacity of the column can be determined for different end conditions according to the iterative method described in step 4 of the simplified procedure proposed in Section 4.2. Axial load capacity for the case with fixed-pinned end conditions and two concrete layers can be calculated as (using Eq. (46) for calculation of $P^*_{axial_i}$'s):

Table 4
$P^*_{critical}$ loads calculated at different strain levels for the tested specimen after 65 min of exposure to the ASTM E119 fire (n: No. of concrete layers).

Load / End conditions / Strain Level	$P^*_{critical}(\varepsilon)$ (kN)			
	Fixed–fixed		Fixed–pinned	
	$n = 2$	$n = 3$	$n = 2$	$n = 3$
$\varepsilon_0 = 0$	2041.2	2034.5	1451.1	1446.7
$\varepsilon_1 - \epsilon = 7.79 \times 10^{-4} - \epsilon$	2026.1	2019.9	1440.5	1436.0
$\varepsilon_1 + \epsilon = 7.79 \times 10^{-4} + \epsilon$	1204.6	1198.4	856.2	851.7
$\varepsilon_2 - \epsilon = 9.33 \times 10^{-4} - \epsilon$	1201.1	1195.3	854.0	849.5
$\varepsilon_2 + \epsilon = 9.33 \times 10^{-4} + \epsilon$	550.5	544.2	391.2	386.7
$\varepsilon_3 - \epsilon = 2.0 \times 10^{-2} - \epsilon$	180.2	178.9	127.7	118.4
$\varepsilon_3 + \epsilon = 2.0 \times 10^{-2} + \epsilon$	97.0	95.7	69.0	68.1
$\varepsilon_4 = 2.5 \times 10^{-2}$	≈ 0	≈ 0	≈ 0	≈ 0

$$P^*_{axial_0} = 0$$
$$i = 1 : P^*_{axial_1} = 21.8 kips < P^*_{critical_2} = 192.4 \text{ kips} \rightarrow i = i + 1 = 2$$
$$i = 2 : P^*_{axial_2} = 25.0 kips < P^*_{critical_4} = 87.9 \text{ kips} \rightarrow i = i + 1 = 3$$
$$i = 3 : P^*_{axial_3} = 118.1 kips > P^*_{critical_5} = 28.7 \text{ kips} :$$
$$P^*_{axial\ capacity} = \frac{P^*_{critical_4} P^*_{axial_3} - P^*_{critical_5} P^*_{axial_2}}{\left(P^*_{axial_3} - P^*_{axial_2}\right) - \left(P^*_{critical_5} - P^*_{critical_4}\right)} = \frac{(87.9)(118.1) - (28.7)(25.0)}{(118.1 - 25.0) - (28.7 - 87.9)} = \frac{10380.9}{152.3} = 68.2 \text{ kips} \quad (58)$$

Note that the calculated capacity (303.4 kN/68.2 kips) is reasonably close to the load values calculated from the analytical solution (following the procedure of Section 4.1) and finite element analysis for the case with fixed-pinned end conditions, which were 306.5 kN and 306.9 kN from Table 3 (68.9, 69.0 kips), respectively. Recall that the specimen, after 65 min of exposure to the ASTM E119 fire curve (the same fire loading condition as the one considered for the calculations above), failed under an axial load of 311.4 kN (70 kips).

To further investigate the accuracy of the simplified solution, experimental results from Lu et al. [14,15] were also considered in investigating behavior of CFDST stub columns subjected to standard fire. The specimen, referred to as "C2-C4-SCC2" in the original paper, was built of outer and inner steel tubes with diameters of 219.1 mm and 165.1 mm, respectively. Wall thickness values were reported as 5 mm for the outer tube and 3.2 mm for the inner tube. Fig. 11a (with solid lines) shows time-history of temperature for three points located on the inner surface of the outer tube, at mid-width of the concrete, and on the outer surface of the inner tube, based on test results presented in the study by Lu et al. [14,15]. The temperature curve recorded for the outer tube was approximated with a piece-wise linear function and used in the simplified heat transfer solution described above for calculation of the temperature field through the thickness of column. Results at points of interest are plotted in Fig. 11a using dashed lines and show good agreement with the experimental data.

Heat transfer results from the simplified solution (shown in Fig. 11a) along with reported yield and maximum compressive strength values of 426 MPa and 63.4 Mpa for steel tubes and infill concrete were used in the procedure presented in Section 4.2 to calculate the axial resistance of specimen during fire. Fig. 11b shows time history of axial displacement recorded for the specimen during the test. The specimen was tested under a constant axial load of 1802 kN with fixed-pinned boundary conditions and failed due to global buckling (shown with extensive axial deformation in Fig. 11b) after about 25–30 min of exposure to fire [14,15]. Results from simplified calculations showed an axial load resistance of about 1650 kN for a 30 min fire exposure, which is slightly less than the test load. The difference can be due to conservative prediction of temperature values as seen in Fig. 11a.

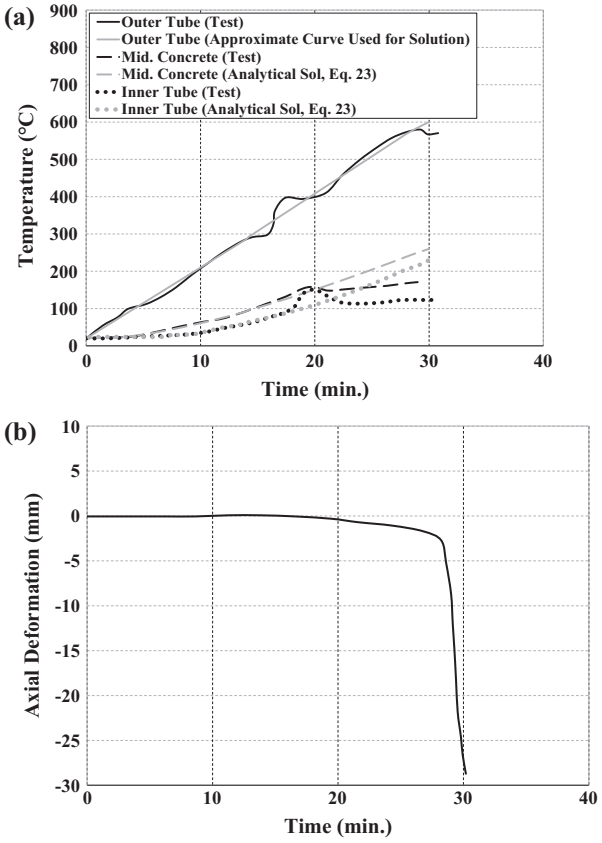

Fig. 11. Results from fire testing of Specimen C2-C4-SCC2: (a) temperature distribution inside the column, test results from Lu et al. [15,16] compared with analytical solution (Eq. (23)); (b) time history of axial deformation [15,16].

The analytical approaches described in this study for calculation of the axial load capacity of CFDST columns subjected to fire were shown to be sufficiently accurate when compared with results from finite element analyses and test data. Although the more sophisticated procedure described in Section 4.1 can provide relatively more accurate results if implemented in a short computer code, the simplified step by step process (presented in Section 4.2) was shown to be capable of providing reasonable axial capacity estimations for design purposes.

It is important to note that the proposed procedure for estimation of axial load capacity of CFDST columns is only verified here against one experiment and requires more extensive validation. Considering the significant assumptions used in the presented

simplified analytical approach (i.e. uniform distribution of strain in the total cross-section, full composite action between the steel and concrete regions, negligible differential expansions, and Euler–Bernouli beam behavior), and the fact that each of these assumptions are possibly contentious, it can be arguably surprising that accurate results were obtained from the simplified method. The reasons for such good agreement are not fully known, and future research may eventually establish why satisfactory results are nonetheless obtained. However, it may be that the equations provide acceptable estimates of the axial load capacity during fire due to the specific boundaries of the column considered here. The CFDST column used in this study (and also the study by Lu et al. [14,15]) was capped with steel plates at its top and bottom ends. Capped ends limit the relative movements at the steel–concrete interfaces and may contribute to develop enough composite action between the steel and concrete region. Proposed the proposed equations might not provide conservative results if: the column ends are not capped and relative movement at the interface is more significant (such as in long columns that can go through significant expansion); or for tubes with large D/t ratios that might lose a considerable amount of their flexural resistance (M_P) due to local buckling.

Another possible explanation is that, after significant fire exposure, little global buckling resistance is provided by the outside tube; however, since the inside tube remains in contact with the concrete (as steel laterally expands more than concrete), most of the initial assumptions remain applicable. Finally, given that the concrete has lost 85% of its strength (and its tangent modulus has reduced to almost zero) by the time global buckling develops, for the verification case considered, the inside tube has a tangent modulus of about 10,684 ksi (71,595 MPa), indicating that the inside tube alone provides most of the flexural strength developed during buckling. This proportion may change when a thicker concrete layer exists between the tubes, which may affect the accuracy of the approximate methods. This remains to be elucidated in future research.

5. Design recommendations for fire resistance of CFDST columns subjected to fire

This section presents general design recommendations to achieve a desired amount of fire resisting time for CFDST columns under axial load. The recommendations are targeted to achieve three levels of fire resistance (under standard ASTM E119 fire), namely 1, 2 and 3 h limits, which each can be sufficient depending on specific applications. The design recommendations are presented separately for the outer tube, concrete core, and inner tube, using the analytical methods described above for both the heat transfer and axial load capacity calculations as needed.

5.1. Inner steel tube

According to the Eurocode specifications for the structural properties of steel at high temperatures (Fig. 5), the temperature of 300 °C can be selected as a critical limit, as the material experiences a decrease of 20% in its elastic modulus and will continue to do so at a significantly higher rate when reaching slightly higher temperatures. Note that the 300 °C limit is also just below the temperature limit for the start of significant reductions in the yield stress of steel (400 °C). In a CFDST column, the inner tube can be thermally protected by the concrete layer to remain below the critical temperature limit for a desired amount of fire exposure time.

Assuming that the minimum required thickness of concrete layer is provided to keep the temperature of the inner tube below the critical limit for the desired amount of fire exposure time (discussed later in Section 5.2), the diameter and thickness of the inner tube can be selected such that (apart from contributing to the pre-fire seismic and service load resistance in other limit states) it can sustain the permanent gravity loads that remain acting on the structure in a post-fire scenario, for the desired fire exposure time. Note that the D/t ratio of the inner tube must be checked to comply with the desired compactness and ductility levels imposed by other limits states (e.g., required by seismic design).

5.2. Concrete core

Concrete has a relatively low heat conductance rate and can act as a fire protection layer for the inner steel tube. Considering the 300 °C limit as the critical temperature for the inner tube, the thickness of the concrete between the inner and outer tube can be chosen such as to delay the inner tube attainment of the critical limit for the desired amount of fire resistance time.

Using the analytical solution presented in Section 3 for the heat transfer problem (specifically Eq. (23)), it is possible to calculate the minimum concrete thickness values required to keep the temperature of inner tubes with diameter sizes ranging from 50.8 mm to 762 mm below the critical limit (i.e., 300 °C) for 1, 2 and 3 h of exposure of the corresponding CFDST column to the standard ASTM E119 fire. Fig. 12a shows the results of these analyses for different fire exposure times. Note that as the inner tube diameter increases, the minimum required concrete layer thickness values converge to a constant limit. This might be explained by looking into a relatively simpler situation where the inner and outer surfaces of a cylinder, with radii of r_1 and r_2, have constant (steady state) temperature values of T_1 and T_2. In this situation, temperature of a point at the distance of r from the center ($r_1 \leqslant r \leqslant r_2$) is proportional to the value $\ln(r/r_1)$ [25]. Assuming r_1 as the radius of the inner tube (equal to the inner radius of the concrete layer), and $r - r_1$ as the thickness of the concrete layer, variation of temperature through the thickness of the concrete layer will be proportional to $\ln(r/r_1)$. Fig. 12b shows the variation of $\ln(r/r_1)$ for different values of inner tube diameter in the range of 50.8 mm to 762 mm ($25.4\ \text{mm} \leqslant r_1 \leqslant 381\ \text{mm}$) and different concrete layer thickness ($r - r_1$) values in the range of 50.8 mm to 152.4 mm. The figure shows that the rate of change in $\ln(r/r_1)$ values decrease as r_1 increases.

Using the plots shown in Fig. 12a, simple equations were defined for the calculation of the minimum required concrete layer thickness as a function of inner tube diameter for different amount of fire exposure time. For a 1-h exposure:

$$t_{min.}^{conc.} = \begin{cases} 25.4(4.90 - 0.20d_{ist}), & 50.8 \leqslant d_{ist} \leqslant 203.2 \\ 16.2, & d_{ist} > 203.2 \end{cases} \quad (59)$$

for a 2-h exposure:

$$t_{min.}^{conc.} = \begin{cases} 25.4(7.40 - 0.25d_{ist}), & 50.8 \leqslant d_{ist} \leqslant 254 \\ 124.5, & d_{ist} > 254 \end{cases} \quad (60)$$

and for a 3-h exposure:

$$t_{min.}^{conc.} = \begin{cases} 25.4(9.30 - 0.20d_{ist}), & 50.8 \leqslant d_{ist} \leqslant 254 \\ 160.0, & d_{ist} > 254 \end{cases} \quad (61)$$

where $t_{min.}^{conc.}$ is the minimum required concrete layer thickness and d_{ist} is the diameter of the inner tube in milimeters. The curves resulting from Eqs. (59)–(61) are plotted with dashed lines on top of the existing curves in Fig. 12a.

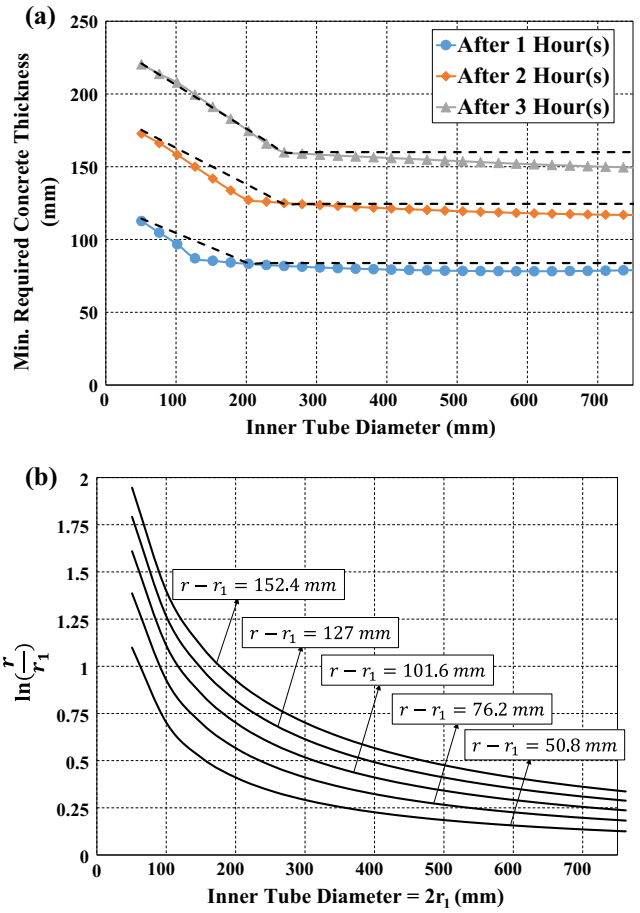

Fig. 12. Applying the analytical heat transfer solution to CFDST columns with different inner tube radius values: (a) minimum concrete thickness required to keep the temperature of inner tube below the critical limit (i.e., 300 C) for 1, 2 and 3 h of exposure to the standard ASTM E119 fire; (b) variation of $ln(\frac{r}{r_1})$ for different values of r_1 and $r - r_1$ (r_1: inner tube radius, $r - r_1$: concrete layer thickness).

5.3. Outer steel tube

The outer tube of a CFDST column subjected to fire reaches the critical temperature level in a relatively short time due to its direct exposure to fire. Note that in the standard ASTM E119 fire curve, the air temperature reaches 300 °C in less than 10 min. Therefore, the outer steel tube will go through significant elastic modulus and yield strength reductions in the early minutes of its fire exposure.

Table 5
Geometric properties of the selected profiles for the outer steel tube.

Code	Profile	Outer diameter (mm)	Thickness (mm)	D/t	Compactness and ductility level
AA	HSS16x0.375	406.4	8.9	45.84	Compact and highly ductile
AB	HSS16x0.438	406.4	10.3	39.31	Compact and highly ductile
AC	HSS16x0.500	406.4	11.8	34.41	Compact and highly ductile
AD	HSS16x0.625	406.4	14.8	27.54	Compact and highly ductile
B	HSS18x0.500	457.2	11.8	38.71	Compact and highly ductile
C	HSS20x0.500	508.0	11.8	43.01	Compact and highly ductile

Considering the situation described above and the fact that the relatively high thermal conductance rate of steel would cause the heat to almost immediately transfer through the thickness of the outer tube, it is inferred that the outer tube has a marginal contribution to the fire resistance of the CFDST columns. Therefore, it is recommended that the minimum required thickness of the outer tube be selected based on the seismic and service load requirements (ignoring the fire performance criteria). For instance, assuming an outer diameter of 381–508 mm for a column used in a typical multistory building, the minimum thickness of the outer tube ($f_y = 345\ \frac{MPa}{50}$ ksi) would need to be 7.4–9.9 mm to satisfy both the compactness and moderate ductility requirements per the AISC seismic specifications [26,27]. Note that the above requirements are for cases where no fire-proofing material is applied to the outer steel, consistently with what has been considered throughout this study.

5.4. Examples: investigating the effect of different section geometry parameters on the axial load capacity of CFDST columns subjected to fire

Different trial cases with outer tube diameters in the range of 381–508 mm (practical sizes for multi-story building columns) were considered to calculate their axial load capacities when subjected to the first 1, 2, and 3 h of the standard ASTM E119 fire. Note that the goal of these examples was not to design a CFDST column for a specific fire performance, but rather to provide a general sense of the axial load capacity of CFDST columns subjected to the standard ASTM E119 fire and study the effects of geometric properties of the section, while the outer diameter size was limited to the range of 381–508 mm and the other remaining parameters

Table 6
CFDST design cases with their calculated axial load capacity.

Case ID.	Outer tube section	Inner tube section	Conc. layer thickness (mm)	Fire exposure time (hour)	Axial load capacity (kN)
1.AA	HSS16.000x0.375	HSS9.625x0.500	72.1	1	1742
1.AB	HSS16.000x0.438	HSS9.625x0.500	70.6	1	1754
1.AC	HSS16.000x0.500	HSS9.625x0.500	69.1	1	1765
1.AD.1	HSS16.000x0.625	HSS9.625x0.250	66.3	1	1213
1.AD.2	HSS16.000x0.625	HSS9.625x0.312	66.3	1	1294
1.AD.3	HSS16.000x0.625	HSS9.625x0.375	66.3	1	1432
1.AD.4	HSS16.000x0.625	HSS9.625x0.500	66.3	1	1788
1.B	HSS18.000x0.500	HSS10.750x0.500	80.3	1	2569
1.C	HSS20.000x0.500	HSS12.750x0.500	80.3	1	3491
2.AD	HSS16.000x0.625	HSS2.875x0.250	151.9	2	833
2.B	HSS18.000x0.500	HSS7.625x0.375	119.9	2	1524
2.C	HSS20.000x0.500	HSS10.000x0.625	115.3	2	2628
3.AD	HSS16.000x0.625	HSS1.660x0.140	167.4	3	332
3.B	HSS18.000x0.500	HSS1.660x0.140	195.8	3	769
3.C	HSS20.000x0.500	HSS3.500x0.313	197.9	3	1581

(i.e., outer tube thickness, concrete layer thickness, and inner tube thickness) were changing.

In the calculations presented here, the outer steel tube is assumed to exactly follow the standard time–temperature curve throughout the fire exposure time. Therefore, the results from these calculation are relatively conservative, because the standard fire curve is defined for the air temperature and the temperature on the surface of the outer steel tube is slightly lower (as seen, for example, in the fire tests results reported in Section 3.3).

Both the outer and inner steel tubes were assumed to have elastic modulus and yield strength values of 29,000 ksi (200,000 MPa) and 42 ksi (290 MPa), respectively. These are nominal values for HSS round sections. A maximum compressive strength of 5 ksi (MPa) was assumed for the concrete. Table 5 shows the geometric properties of the different round HSS section selected for the outer steel tubes.

To study the effect of concrete thickness, different cases, ranging from a minimum thickness of 50.8 mm up to a maximum of 177.8 mm, were checked for all of the outer tube sections specified in Table 5 using Eq. (23), with the goal of keeping the inner tube temperature below the critical limit (300 °C) at the end of the 1, 2 and 3-h fire exposures. Fig. 13a shows the results of the inner tube temperatures calculated for a CFDST column with the outer tube section AA (from Table 5) for different values of concrete thicknesses (ranging from 50.8 to 177.8 mm), after 1, 2 and 3 h of exposure to the ASTM E119 fire curve.

Looking into Fig. 13a, there are two cases for the 1-h fire exposure time in which the inner tube temperature was kept below the critical limit. These cases have concrete thickness values of 101.6 mm and 127.0 mm for inner tubes with outer diameters of 203.2 mm and 152.4 mm, respectively. Note that both of the mentioned concrete layer thickness values are above the minimum required value calculated using Eq. (59) for inner tube with the mentioned diameter sizes (the calculated minimum thickness values were equal to 83.8 and 94.0 mm). Fig. 13a also shows that a CFDST column with the outer tube diameter of 406.4, regardless of the geometric properties of the inner tube and concrete layer, will not be able to keep the temperature of its inner tube below the critical limit for a 3-h period. This is because selection of an inner tube with the smallest available diameter size ($d_{ist} = 42.2mm$) results in the thickness value of 173.2 mm for the concrete layer, which is not sufficient.

Using the outer tube sections shown in Table 5 total of 15 CFDST column cross-sections were defined to be used in the axial load capacity calculation for different fire exposure times. Table 6 shows all of the selected cases with their axial load capacity values calculated using the simplified analytical step by step method described in Section 4.2. All of the columns are assumed to have a length of 4064 mm (typical story height) and pinned–pinned boundary conditions. The inner tube sections were selected such as to create cases with different concrete layer thickness and inner tube thickness values. Note that design cases 1.AD.1 to 1.AD. 4 are selected to assess the effects of changes in the inner tube thickness on the axial load capacity of the column when all of the other geometric parameters are kept constant. Also cases 1.AA, 1.AB, 1.AC and 1.AD.4 are selected to perform a similar analysis on the outer tube thickness (with marginal changes in the concrete layer thickness). For cases in which only one thickness is chosen for the inner or outer tube, it was taken to be equal to the maximum available thickness (based on shapes listed in the AISC Steel Construction Manual).

Fig. 13b shows the effect of changes in the thickness of outer and inner tubes on the axial load capacity of CFDST columns subjected to the first hour of the standard ASTM E119 fire. Note that the changes are made to a base model with an axial load capacity of about 1779 kN (400 kips), for which all other geometric parameters are kept constant. The figure shows that changes in the outer tube thickness do not significantly affect the axial load capacity of the column. On the other hand, increasing the thickness of the inner tube has increased the axial load capacity by as much as 32% in the cases considered. The difference is due to the fact that the inner tube temperature remains significantly lower than that of the outer tube and increasing the thickness of the former leads to a significant increase in the column's axial load capacity.

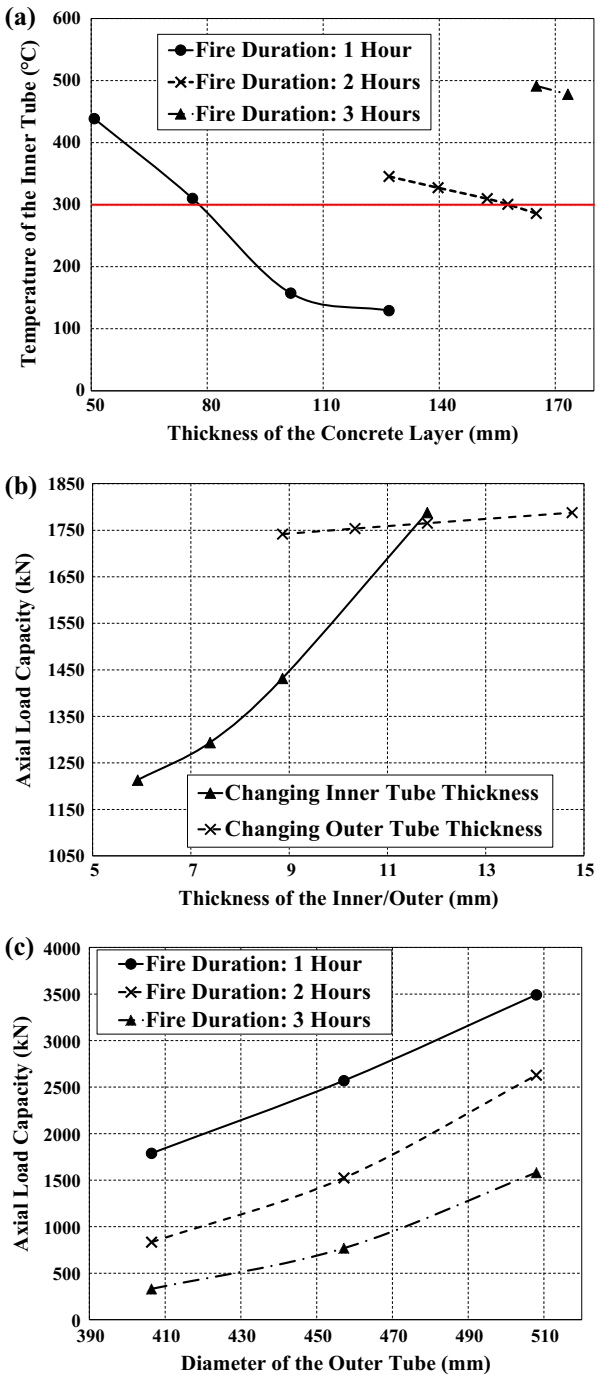

Fig. 13. Effects of the section geometry on the behavior of CFDST columns subjected to the ASTM E119 fire: (a) inner tube temperature for varying concrete thickness; (b) axial load capacity of columns with varying inner and outer tube thickness values; (c) axial load capacity of columns with varying outer diameter for cases optimized for all other parameters.

Fig. 13c shows the effects of changes in the outer tube diameter on the axial load capacity of CFDST columns, assuming that all of the other section geometric properties are selected such as to maximize the axial resistance after the start of fire. The axial load capacity increases for larger outer tube diameters in a similar trend for all of the three fire duration choices. The results were expected, since increasing the diameter of the outer tube allows for the selection of larger concrete layer thickness, which can generally enhance the column's performance under fire.

6. Conclusions

An analytical procedure was developed for the calculation of the axial load capacity of CFDST columns subjected to fire. The procedure started with a solution for the heat transfer problem, derived analytically by solving the partial differential equation of heat conduction. The solution was simplified to an explicit formula that can provide the temperature of any point in the CFDST column's cross-section, after a given amount of exposure time to any predefined time–temperature curve. The simplification process had a marginal conservative effect on the accuracy of the calculation that resulted in slightly higher temperature values as a consequence of replacing a few temperature dependent factors with constant values recommended in the Eurocode 4. Comparing with experimental and finite element results, the temperature values calculated using the simplified analytical formula were shown to be sufficiently accurate.

The second part of the analytical procedure consisted of a simplified step by step method to estimate the axial load capacity of CFDST columns subjected to fire using the temperature modified material properties calculated in the previous part. The method is based on solving for axial equilibrium using simple expressions for the structural material properties at elevated temperatures. Calculated results were in good agreement with the finite element and experimental results for a previously tested specimen.

The analytical procedure defined for the axial load capacity calculation was applied to a few case studies to propose some general design recommendations for axially loaded CFDST columns subjected to fire. It was suggested that to retain a given axial load for a certain amount of time, the most effective solution is to design an inner tube capable of sustaining that load and make the concrete layer thick enough to keep the inner tube's temperature below the critical limit (about 300 °C) for the specified amount of fire resistance time.

Moreover, it was found that for a given CFDST column cross-section (i.e., known diameters of the inner and outer tubes), changes in the thickness of the outer tube do not significantly affect the column's axial load capacity after a certain amount of exposure to fire. Changing the thickness of the inner tube, on the other hand, can be significantly effective, because, being at much lower temperatures than the outer tube, its capacity is retained for a longer time. Additional calculations confirmed the intuitive expectation that increasing the diameter of the outer tube, or any other change that results in a thicker concrete layer, generally increases the axial load capacity of CFDST columns subjected to fire.

Appendix A. Solution to the heat transfer equation for a circular section subjected to the fire curve, $f(t)$, around the outer edge and simplification for a bilinear $f(t)$

This appendix presents the solution for the differential equation given in Eq. (14) of the main text. The solution is as follows:

$$\alpha^2\left(v_{,rr}+\frac{1}{r}v_{,r}\right)=v_{,t}+f'(t)\quad 0=r_i\leqslant r\leqslant r_o,\ 0\leqslant t<\infty$$
$$v(r,0)=0,\quad v(r_o,t)=0 \tag{14}$$

Note that the new problem has a homogeneous boundary condition, but the differential equation itself has changed to a non-homogeneous one because of the addition of the term, $f'(t)$. Assuming the function, v, as a summation of its homogeneous and particular parts $(v=v_h+v_p)$, and using the method of Separation of Variables, the homogeneous part of the solution for the differential equation can be written solved for as follows:

$$v_h(r,t)=R(r)T(t) \tag{A.1}$$

$$\frac{R_{,rr}+\frac{1}{r}R_{,r}}{R}=\frac{1}{\alpha^2}\frac{T_{,t}}{T}=constant=-\kappa^2 \tag{A.2}$$

$$R_{,rr}+\frac{1}{r}R_{,r}+\kappa^2R=0 \tag{A.3}$$

$$T_{,t}+\kappa^2\alpha^2T=0 \tag{A.4}$$

$$R(r)=\begin{cases}C_1J_0(\kappa r)+C_2Y_0(\kappa r), & \kappa\neq 0\\ C_3+C_4ln(r), & \kappa=0\end{cases} \tag{A.5}$$

$$T(t)=\begin{cases}C_5e^{-\kappa^2\alpha^2t}, & \kappa\neq 0\\ C_6, & \kappa=0\end{cases} \tag{A.6}$$

$$\begin{aligned}v_h(r,t)&=[C_3+C_4\ln(r)]C_6+[C_1J_0(\kappa r)+C_2Y_0(\kappa r)]C_5e^{-\kappa^2\alpha^2t}\\&=C_1'+C_2'\ln(r)+[C_3'J_0(\kappa r)+C_4'Y_0(\kappa r)]e^{-\kappa^2\alpha^2t}\end{aligned} \tag{A.7}$$

Note that, aside from the boundary condition given in the Eq. (14), it is appropriate to require that v_h must be bounded at $r=0$. This is a reasonable requirement, since the temperature at r_i starts from the room condition and will increase to some extent according to the given fire curve. Considering the nature of the fire curves, the final temperature value at $r=0$ will eventually reach a limit (which will be less than the maximum outer tube temperature). Applying this limit condition (as a boundary) at $r=0$ requires that:

$$\begin{aligned}v_h(0,t)&=C_1'+C_2'\ln(r)+[C_3'J_0(\kappa r)+C_4'Y_0(\kappa r)]e^{-\kappa^2\alpha^2t}\\&\rightarrow bounded\end{aligned} \tag{A.8}$$

Since both $ln(r)$ and $Y_0(\kappa r)$ are unbounded at $r=0$, in order to satisfy Eq. (A.8), the constants C_2' and C_4' must be equal to zero. Eq. (A.7) simplifies to:

$$v_h(r,t)=C_1'+C_3'J_0(\kappa r)e^{-\kappa^2\alpha^2t} \tag{A.9}$$

Applying the other boundary condition, $v_h(r_o,t)=0$, to Eq. (A.9) gives:

$$v_h(r_o,t)=C_1'+C_3'J_0(\kappa r_o)e^{-\kappa^2\alpha^2t}=0\ \text{for}\ 0\leqslant t<\infty \tag{A.10}$$

Since C_1' (as a constant) and $C_3'J_0(\kappa r_o)e^{-\kappa^2\alpha^2t}$ are linearly independent in the t interval, it follows from Eq. (A.10) that $C_1'=0$ and $C_3'J_0(\kappa r_o)=0$. The latter gives $C_3'=0$ or $J_0(\kappa r_o)=0$. Since the elimination of the $C_3'J_0(\kappa r_o)e^{-\kappa^2\alpha^2t}$ term would lead to a trivial solution, it is inferred that:

$$J_0(\kappa r_o)=0 \tag{A.11}$$

The solution for Eq. (A.11) consists of positive roots of the J_0 function that are referred to as $z_n=\kappa_n r_o$ (these roots are known and will be used later). Using superposition and substituting C for C_3' for simplicity, the homogenous part of the solution for the differential equation becomes:

$$v_h=\sum_{n=1}^{\infty}C_nJ_0\left(z_n\frac{r}{r_o}\right)e^{-\left(\frac{z_n\alpha}{r_o}\right)^2t} \tag{A.12}$$

where the C_n's are constants. Now the particular solution, v_p, needs to be added to v_h. Taking v_p as:

$$v_p = \sum_{n=1}^{\infty} D_n(t) J_0\left(z_n \frac{r}{r_o}\right) e^{-\left(\frac{z_n \alpha}{r_o}\right)^2 t} \tag{A.13}$$

where $D_n(t)$ is a function of only $t$and Substituting it into Eq. (14) gives:

$$\alpha^2 \left(v_{p_{rr}} + \frac{1}{r} v_{p_r}\right) = v_{p_t} + f'(t) \tag{A.14}$$

$$\sum_{n=1}^{\infty} D'_n(t) J_0\left(z_n \frac{r}{r_o}\right) e^{-\left(\frac{z_n \alpha}{r_o}\right)^2 t} = -f'(t) \tag{A.15}$$

which is in the Bessel-Fourier series form. Multiplying both sides of Eq. (A.16) by the term $\frac{r}{r_o} J_0(z_m \frac{r}{r_o})$ and integrating in the domain $0 = r_i < r < r_o$ gives:

$$\int_0^{r_0} \frac{r}{r_o} J_0\left(z_m \frac{r}{r_o}\right) \sum_{n=1}^{\infty} D'_n(t) J_0\left(z_n \frac{r}{r_o}\right) e^{-\left(\frac{z_n \alpha}{r_o}\right)^2 t} dr = \int_0^{r_o} (-f'(t)) \frac{r}{r_o} J_0\left(z_m \frac{r}{r_o}\right) dr \tag{A.16}$$

Using the orthogonallity of Bessel functions, Eq. (A.16) is simplified to:

$$\int_0^{r_0} \frac{r}{r_o} D'_n(t) J_0^2\left(z_n \frac{r}{r_o}\right) e^{-\left(\frac{z_n \alpha}{r_o}\right)^2 t} dr = \int_0^{r_o} (-f'(t)) \frac{r}{r_o} J_0\left(z_n \frac{r}{r_o}\right) dr \tag{A.17}$$

Using:

$$\int s J_0(s) ds = s J_1(s) + C \tag{A.18}$$

$$\int_0^a s \left[J_v^2(z_n s)\right] ds = \frac{a^2}{2} \left[J_{v+1}^2(z_n a)\right] \tag{A.19}$$

On Eq. (A.17) gives:

$$D'_n(t) = \frac{2(-f'(t))}{z_n J_1(z_n)} e^{\left(\frac{z_n \alpha}{r_o}\right)^2 t} \tag{A.20}$$

$$D_n(t) = \int_0^t D'_n(\tau) d\tau = \int_0^t \frac{2(-f'(\tau))}{z_n J_1(z_n)} e^{\left(\frac{z_n \alpha}{r_o}\right)^2 \tau} d\tau \tag{A.21}$$

in which $f'(t)$ is the derivative of the predetermined time–temperature (fire) curve, which is applied to the outer edge of the section. Now summing up the homogeneous and particular solutions ($v = v_h + v_p$) gives:

$$v = v_h + v_p = \sum_{n=1}^{\infty} [C_n + D_n(t)] J_0\left(z_n \frac{r}{r_o}\right) e^{-\left(\frac{z_n \alpha}{r_o}\right)^2 t} = \sum_{n=1}^{\infty} \left[C_n + \int_0^t \frac{2(-f'(\tau))}{z_n J_1(z_n)} e^{\left(\frac{z_n \alpha}{r_o}\right)^2 \tau} d\tau\right] J_0\left(z_n \frac{r}{r_o}\right) e^{-\left(\frac{z_n \alpha}{r_o}\right)^2 t} \tag{A.22}$$

Satisfying the initial boundary condition ($v(r,0) = 0$) gives:

$$v(r,0) = \sum_{n=1}^{\infty} [C_n + D_n(0)] J_0\left(z_n \frac{r}{r_o}\right) e^{-\left(\frac{z_n \alpha}{r_o}\right)^2 (0)} = \sum_{n=1}^{\infty} \left[C_n + \int_0^0 \frac{2(-f'(\tau))}{z_n J_1(z_n)} e^{\left(\frac{z_n \alpha}{r_o}\right)^2 \tau} d\tau\right] J_0\left(z_n \frac{r}{r_o}\right) = \sum_{n=1}^{\infty} C_n J_0\left(z_n \frac{r}{r_o}\right) = 0 \tag{A.23}$$

from which it is inferred that $C_n = 0$ (since $J_0(z_n \frac{r}{r_o}) \neq 0$). Finally, the solution for the temperature field in the circular section, $u(r,t)$, can be written as:

$$u(r,t) = v(r,t) + u_0(r,t)$$

$$u(r,t) = \left[\sum_{n=1}^{\infty} \underbrace{\left[\int_0^t \frac{2(-f'(\tau))}{z_n J_1(z_n)} e^{\left(\frac{z_n \alpha}{r_o}\right)^2 \tau} d\tau\right]}_{I^*} J_0\left(z_n \frac{r}{r_o}\right) e^{-\left(\frac{z_n \alpha}{r_o}\right)^2 t}\right] + f(t) \tag{A.24}$$

Assuming that the function, $f(t)$, is bilinear, the integral term in Eq. (A.22) can be computed as:

$$\int_0^t \frac{2(-f'(\tau))}{z_n J_1(z_n)} e^{\left(\frac{z_n \alpha}{r_o}\right) \tau} d\tau = \frac{-2}{z_n J_1(z_n)} \begin{cases} \left[a_1 \int_0^t e^{\left(\frac{z_n \alpha}{r_o}\right)^2 \tau} d\tau\right], & t \leqslant t_1 \\ \left[a_1 \int_0^{t_1} e^{\left(\frac{z_n \alpha}{r_o}\right)^2 \tau} d\tau + a_2 \int_{t_1}^{t_2} e^{\left(\frac{z_n \alpha}{r_o}\right)^2 \tau} d\tau\right], & t > t_1 \end{cases} \tag{A.25}$$

After computing the integral terms, Eq. (A.23) can be written as:

$$\int_0^t \frac{2(-f'(\tau))}{z_n J_1(z_n)} e^{\left(\frac{z_n \alpha}{r_o}\right) \tau} d\tau = \frac{-2r_o^2}{\alpha^2 z_n^3 J_1(z_n)} \begin{cases} a_1 \left[e^{\left(\frac{z_n \alpha}{r_o}\right)^2 t} - 1\right], & t \leqslant t_1 \\ a_1 \left[e^{\left(\frac{z_n \alpha}{r_o}\right)^2 t_1} - 1\right] + a_2 \left[e^{\left(\frac{z_n \alpha}{r_o}\right)^2 t} - e^{\left(\frac{z_n \alpha}{r_o}\right)^2 t_1}\right], & t > t_1 \end{cases} \tag{A.26}$$

according to which, the function $A_n(t)$ can be defined as:

$$A_n(t) = \begin{cases} a_1 \left[e^{\left(\frac{z_n \alpha}{r_o}\right)^2 t} - 1\right], & t \leqslant t_1 \\ a_1 \left[e^{\left(\frac{z_n \alpha}{r_o}\right)^2 t_1} - 1\right] + a_2 \left[e^{\left(\frac{z_n \alpha}{r_o}\right)^2 t} - e^{\left(\frac{z_n \alpha}{r_o}\right)^2 t_1}\right], & t > t_1 \end{cases} \tag{A.27}$$

Note that, only the first four terms of $A_n(t)$ are needed (using the constants z_1 to z_4) for a sufficiently accurate result. Therefore, solution of the differential equation for a bilinear $f(t)$ can be written as:

$$u_{bilinear\ fire}(r,t) = \left[\sum_{n=1}^{4} \frac{-2r_o^2 A_n(t)}{\alpha^2 z_n^3 J_1(z_n)} J_0\left(z_n \frac{r}{r_o}\right) e^{-\left(\frac{z_n \alpha}{r_o}\right)^2 t}\right] + f(t) \tag{A.28}$$

Using the numerical values of $J_1(z_n)$ for the first four terms, the approximate formula for the calculation of $J_0(z)$ (Eq. (17)), the resulting equation is:

$$u_{bilinear\ fire}(r,t) = \frac{r_o^2}{\alpha^2} [-0.2770 A_1(t) B_1(t) + 0.0349 A_2(t) B_2(t) - 0.0114 A_3(t) B_3(t) + 0.0052 A_4(t) B_4(t)] + f(t) \tag{A.29}$$

References

[1] Hajjar JF. Concrete-filled steel tube columns under earthquake loads. Prog Struct Eng Mater 2000;2(1):72–81.
[2] Marson J, Bruneau M. Cyclic testing of concrete-filled circular steel bridge piers having encased fixed-based detail. J Bridge Eng 2004;9(1):14–23.
[3] Han LH, Yang YF. Cyclic performance of concrete-filled steel CHS columns under flexural loading. J Constr Steel Res 2005;61(4):423–52.
[4] CEN, Eurocode 4: design of composite steel and concrete structures, part 1.2: general rules – structural fire design. Brussels, Belgium: Comité Européen de Normalisation; 2005.
[5] Kodur VKR. Performance of high strength concrete-filled steel columns exposed to fire. Can J Civil Eng 1998;25(6):975–81.
[6] Han LH. Fire performance of concrete filled steel tubular beam-columns. J Constr Steel Res 2001;57(6):695–709.
[7] Han LH, Zhao XL, Yang YF, Feng JB. Experimental study and calculation of fire resistance of concrete-filled hollow steel columns. ACSE J Struct Eng 2003;129(3):346–56.
[8] Hong S, Varma AH. Analytical modeling of the standard fire behavior of loaded CFT columns. J Constr Steel Res 2009;65(1):54–69.
[9] Moliner V, Espinos A, Romero ML, Hospitaler A. Fire behavior of eccentrically loaded slender high strength concrete-filled tubular columns. J Constr Steel Res 2013;83:137–46.
[10] Zhao XL, Grzebieta R. Strength and ductility of concrete filled double skin (SHS inner and SHS outer) tubes. Thin Wall Struct 2002;40(2):199–213.

[11] Han LH, Tao Z, Huang H, Zhao XL. Concrete-filled double skin (SHS outer and CHS inner) steel tubular beam-columns. Thin Wall Struct 2004;42(9):1329–55.
[12] Uenaka K, Kitoh H, Sonada K. Concrete filled double skin tubular members subjected to bending. Steel Comp Struct 2008;8(5). 439-439.
[13] Yang YF, Han LH. Concrete-filled double-skin tubular columns under fire. Mag Concrete Res 2008;60(3):211–22.
[14] Lu H, Han LH, Zhao XL. Testing of self-consolidating concrete-filled double skin tubular stub columns exposed to fire. J Constr Steel Res 2010;66(8):1069–80.
[15] Lu H, Zhao XL, Han LH. FE modelling and fire resistance design of concrete filled double skin tubular columns. J Constr Steel Res 2011;67(11):1733–48.
[16] Imani R, Mosqueda G, Bruneau M. Experimental study on post-earthquake fire resistance of ductile concrete filled double-skin tube columns. ASCE J Struct Eng 2014. http://dx.doi.org/10.1061/(ASCE)ST.1943-541X.0001168.
[17] Kodur VKR, MacKinnon DH. Simplified design of concrete-filled hollow structural steel columns for fire endurance. J Constr Steel Res 1998;46(1–3):298.
[18] Espinos A, Romero ML, Hospitaler A. Simple calculation model for evaluating the fire resistance of unreinforced concrete filled tubular columns. Eng Struct J 2012;42:231–44.
[19] ASTM, E119-12a: standard test methods for fire tests of building construction and materials. West Conshohocken, PA: ASTM International; 2012.
[20] Greenberg MD. Advanced engineering mathematics. Pearson Education; 1998.
[21] Imani R, Mosqueda G, Bruneau M. post-earthquake fire resistance of ductile concrete-filled double-skin tube columns. MCEER Tech. Rep. no. MCEER-14-0008, Buffalo, NY: MCEER 2014. <http://mceer.buffalo.edu/publications/catalog/reports/Post-Earthquake-Fire-Resistance-of-Ductile-Concrete-Filled-Double-Skin-Tube-Columns-MCEER-14-0008.html>.
[22] Imani R, Mosqueda G, Bruneau M. Finite element simulation of concrete-filled double-skin tube columns subjected to postearthquake fires. ASCE J Struct Eng 2015. http://dx.doi.org/10.1061/(ASCE)ST.1943-541X.0001301.
[23] Hognestad E. A study on combined bending and axial load in reinforced concrete members. Univ. of Illinois at Urbana-Champaign, IL: Univ. of Illinois Engineering Experiment Station; 1951. p. 43–6.
[24] Hjelmstad KD. Fundamentals of structural mechanics. Springer; 2005.
[25] Sukhatme SP. A textbook on heat transfer. Universities Press; 2005.
[26] AISC, ANSI/AISC 360-10: specification for structural steel buildings. Chicago, IL: American Institute of Steel Construction; 2010.
[27] AISC, ANSI/AISC 341-10: seismic provisions for structural steel buildings. Chicago, IL: American Institute of Steel Construction; 2010.